School of Computing, Engineering and Built Environment

Department of Electrical and Electronic Engineering

EEE Honours Research Project

MHH630296

BEng Electrical and Electronic Engineering

Simulation of Multi-beam Antenna Array

By

Lewis Mitchell

Supervisor: Sinan Sinanovic

Abstract

The sudden spike of Low Earth Orbit (LEO) satellites such as Starlink and OneWeb along with the recent increase of Very Low Earth Orbit (VLEO) missions means an increase in the need for supporting systems. Moving from traditional mechanical antennas to phased array antennas opened the ability to track accurately with electronic steering and beamforming but now systems are getting much more complex with the modern demands.

This project developed a simulation framework in MATLAB to model phased array beamforming with a focus on LEO satellite tracking. The final simulation used key parameters for a uniform rectangular array and has the ability to generate multiple beams to track targets simultaneously. Along with the addition of real satellite orbital data taken from TLE files and live SNR calculations. This allowed the study of different parameters to assist in the design process.

The results showed that the simulation framework is functional and adequate for performing basic testing. If a full simulation is developed the applications could be vast, removing cost and time of designing the complex modern systems needed today.

Acknowledgements

The author would like to thank Dr. Sinan Sinanovic for his helpful advice. Thanks, are also given to the M330 lab room, which provided a good space for working and testing.

Contents

nomenclature

Abbreviation	Full Meaning
LEO	Low Earth Orbit
SNR	Signal-to-Noise Ratio
TLE	Two-Line Element (Satellite Data Format)
RF	Radio Frequency
HPBW	Half Power Beamwidth
2D	Two-Dimensional
3D	Three-Dimensional
dB	Decibel
dBi	Decibel relative to isotropic radiator
Tx	Transmitter
Rx	Receiver
AoA	Angle of Arrival
FFT	Fast Fourier Transform
AF	Array Factor
CPU	Central Processing Unit
MATLAB	Matrix Laboratory (Software Environment)

Symbol	Units	Description
f	Hz	Operating frequency of the antenna array
λ	m	Wavelength corresponding to the operating frequency
k	rad/m	Wavenumber, defined as $k=2\pi/\lambda$
M	—	Number of elements along the X-axis
N	—	Number of elements along the Z-axis
d_x	m	Spacing between adjacent elements along the X-axis
D_z	m	Spacing between adjacent elements along the Z-axis
θ	degrees	Elevation angle from the positive Z-axis
ϕ	degrees	Azimuth angle from the X-axis
θ_s	degrees	Desired steering elevation angle
ϕ_s	degrees	Desired steering azimuth angle
ψ_x	radians	Phase shift for elements along the X-axis
ψ_z	radians	Phase shift for elements along the Z-axis
AF	—	Total 2D array factor
AF_X	—	1D array factor along the X-axis
AF_Z	—	1D array factor along the Z-axis
B	—	Number of beams tracked simultaneously
AF_b	—	Array factor of the b-th beam
R	—	Magnitude of the radiation pattern
x,y,z	m	Cartesian coordinates in the radiation plot
P_r	W	Received power
P_t	W	Transmitted power
G_t	dBi	Gain of the transmitting antenna
G_r	dBi	Gain of the receiving antenna
d	m	Distance between satellite and ground station
SNR	dB	Signal-to-noise ratio

1 Introduction

The rapid growth of Low Earth Orbit (LEO) satellite constellations, such as Starlink and OneWeb, along with the increase in Very Low Earth Orbit (VLEO) missions, has created a higher demand for supporting systems. Traditional ground antennas use mechanical movement, which is slow and wears out over time. These limitations cause major problems when tracking fast-moving LEO satellites. Phased array antennas offer a strong alternative. By electronically steering beams through controlled phase shifts across multiple antenna elements, they eliminate the need for mechanical motion. Phased arrays also allow for accurate tracking, simultaneous multi-satellite coverage, and dynamic beam reconfiguration. However, meeting modern demands has increased the complexity of these systems.

Although the technology adds the ability for rapid electronic steering it introduces more challenges. Some examples being controlling side lobes, minimising beam squint and keeping a strong signal to noise ratio (SNR) over angles far away from boresight.

This project developed a simulation framework in MATLAB to model phased array beamforming for LEO satellite tracking. The simulation used key parameters for a uniform rectangular array and added the ability to generate multiple beams aimed at different azimuth and elevation targets. Real satellite orbital data from Two-Line Element (TLE) files and live signal-to-noise ratio (SNR) calculations were also integrated into the framework. These additions allowed detailed study of how array design choices affect tracking performance and system capabilities.

The results show that the simulation framework is functional and capable of basic system testing. The project successfully created a flexible base that can support real-time satellite tracking and advanced performance analysis in future work. Expanding the simulation could significantly reduce the time and cost needed to design complex, modern satellite tracking systems.

1.1 Aim(s) of the Project

The original aim of this project was to show the benefits of phased arrays for satellite tracking. The project planned to compare phased arrays with traditional parabolic dish antennas. Phased arrays have clear advantages, including faster movement, higher

reliability, and multi-satellite tracking. As the project continued, the limits of simple comparisons became clear. Phased arrays already outperform dishes in tracking Low Earth Orbit (LEO) satellites. Because of this, the project focus shifted to a more forward-looking goal.

The new aim was to design, simulate, and test multi-beam phased array systems using MATLAB. This change allowed deeper study of beamforming, tracking accuracy, and phased array challenges. It also helped build a stronger base for future real-time tracking with satellite orbit data. The revised aim of the project is to test how well multi-beam phased arrays can track LEO satellites. A modular MATLAB simulation was developed to explore system design, performance, and future growth.

1.2 Objectives of the Project

1. Review relevant literature on phased array antenna systems, beamforming techniques, and LEO satellite tracking to establish a strong theoretical foundation.
2. Develop and implement a simulation of single-beam steering using a uniform rectangular array to validate directional control through phase manipulation.
3. Extend the simulation framework to support simultaneous multi-beam steering for tracking multiple satellites at distinct azimuth and elevation angles.
4. Evaluate the influence of array parameters—including frequency, element spacing, and array size—on beamwidth, gain, and directional accuracy.
5. Design the system to allow future real-time tracking using TLE orbit prediction, with beam selection based on updated link quality.

1.3 Scope of the Project

This project focuses on simulating and testing phased array antennas for Low Earth Orbit (LEO) tracking. The work builds a MATLAB simulation that models both single-beam and multi-beam steering. The simulation studies how array size, element spacing, and frequency affect beam direction and resolution.

The main goal is to test the basic principles of phased array beamforming in ideal conditions.

Two main programs were created: one to steer a single beam and one to form multiple beams. Each beam can aim at different azimuth and elevation angles to track several satellites at once. The system can also accept and organize Two-Line Element (TLE) data for future orbit tracking upgrades. This prepares the simulation for later use with

dynamic satellite positioning. Real-time TLE orbit updates are planned for future versions but were not added here. Certain features were not included in the project to keep the scope focused. Real-time orbit propagation with SGP4, hardware testing, and full link budgeting were excluded. Dynamic SNR adjustment and power efficiency analysis were also left out to simplify the work. The simulation models beam steering and spatial resolution under perfect conditions only. It does not model real-world effects like weather, interference, atmospheric loss, or Doppler shifts. These real-world factors will be important to add in future work for practical systems. Several assumptions were made to support the simple design. The project uses ideal, lossless antenna elements, half-wavelength spacing, and static targets. The work also assumes free-space propagation without environmental signal loss or degradation.
Even with these limits, the project follows a systems-based approach with modular design. This makes it easier to expand later into real-time control, environmental modelling, and closed-loop tracking.

1.4 Structure of the Report

The report takes the reader from background research to the final conclusions. Each section builds step-by-step, showing how the project was planned, tested, and improved.
Chapter 1 – Introduction: Describes the project background and the main goals. Lists the problem being solved and the scope. Explains how the report is organised.
Chapter 2 – Literature Review: Reviews key topics like phased arrays, beamforming, and satellite tracking. Shows research gaps in past studies. Explains how this project adds new ideas.
Chapter 3 – Background and Theoretical Framework: Covers the basic theory of phased arrays and beam steering. Introduces the MATLAB simulation tools used. Explains important models used in the project.
Chapter 4 – Methodology and Implementation: Describes how the simulation system was designed and built. Shows how single-beam and multi-beam models were created. Explains how the system was tested.
Chapter 5 – Simulations and Analysis: Presents the simulation results. Includes beam patterns, performance checks, and tests with different settings.

Chapter 6 – Discussion and Critical Evaluation: Explains the meaning of the results. Discusses the system's good points and problems. Suggests ways to fix or improve the system.
Chapter 7 – Conclusions and Future Work: Summarizes the key results of the project. Recommends ways to improve the simulation.

.

2 Literature Review

The design and use of electronically steerable phased arrays for LEO satellite tracking relies on several research fields. These fields include antenna theory, satellite communication, and orbital dynamics. The rapid growth of satellite networks and global communication needs has made phased arrays more important than ever. Antenna arrays, especially phased arrays, are now a main area of study in RF engineering. Engineers in systems, software, and aerospace roles are increasingly solving RF-related problems in new projects. Wireless communication has expanded so much that many engineering teams now require RF knowledge to succeed. Understanding phased array behaviour and knowing how to simulate performance are strong skills today. Engineers with these skills are valuable in multidisciplinary teams that work across many fields. This project aims to meet industry needs by offering a flexible, modular phased array simulation tool for future research.
This section reviews important developments related to phased arrays and satellite tracking technology. The review focuses on basic phased array concepts while identifying gaps that still exist in research. These gaps define the technical focus and development goals of this project.

2.1 Satellite Tracking in Low Earth Orbit

Low Earth Orbit (LEO) is typically defined as the region up to about 2,000 km above Earth's surface, with most LEO satellites orbiting at a few hundred kilometres altitude [1]. At these heights, satellites circle the Earth extremely fast – for example, the International Space Station at ~400 km altitude travels about 27,600 km/h and completes roughly 16 orbits per day [1]. This high orbital speed means any given LEO satellite is only in view of a fixed ground point for a short duration (often 5–15

minutes per pass). Unlike geostationary satellites (which remain fixed relative to an Earth location), LEO satellites sweep rapidly across the sky and can have inclined or polar orbits instead of being limited to the equatorial plane [1], [2]. This orbital agility makes LEO attractive for many applications – including Earth imaging, scientific missions, and low-latency communications – but it also poses a major tracking challenge for ground stations.

A single LEO satellite cannot provide continuous coverage to one ground location, so operators deploy large constellations of many satellites to achieve global or near-continuous coverage [2]. Recent years have seen an explosion in such LEO constellations. Notably, SpaceX's Starlink constellation has grown to over 7,000 satellites in orbit as of early 2025 [2], and networks like OneWeb are also operational. This dramatic increase in LEO spacecraft has amplified the demand for real-time, scalable tracking solutions. Traditional ground tracking systems typically use large parabolic dish antennas mounted on mechanical gimbals. While mechanically steered dishes work well for slowly moving geostationary targets, they struggle to keep pace with fast-moving LEO satellites that traverse from horizon to horizon in minutes. Mechanical systems have inherent slewing speed limits and wear over time due to moving parts. They are also limited to tracking one satellite at a time. Handling dozens or hundreds of simultaneous LEO passes would require an impractical number of dish antennas or extremely rapid retargeting between satellites. Recent studies and industry roadmaps emphasize that new approaches are needed to track multiple LEO objects in real time [3]. NASA's small satellite communications roadmap highlights electronically steered array antennas as a key emerging solution to enable simultaneous links to many LEO satellites [3]. In summary, the proliferation of LEO constellations has created an urgent need for ground station technologies that can rapidly steer, and even simultaneously split antenna beams to follow multiple satellites. This sets the stage for modern phased array antenna systems.

2.2 Phased Array Antenna Systems

Phased array antennas have been studied for decades as a compelling alternative to mechanically steered dishes for high-speed tracking and communications. A phased array consists of many small radiating elements arranged in an array and driven with carefully adjusted phase shifts. By controlling the relative phase and amplitude of the signal at each element, the array's combined radiation pattern can be electronically

steered in desired directions without any mechanical movement [4], [5]. This principle was pioneered in radar systems in the mid-20th century to track airborne targets and missiles much faster than any dish antenna could slew [5]. Classic antenna theory texts such as Balanis and Mailloux provide the mathematical foundations for phased arrays, demonstrating how a uniformly excited array can produce a narrow main lobe and low sidelobes by appropriate phasing and weighting of elements [4], [5]. For example, a planar array of many elements can achieve a beamwidth of only a few degrees or less, concentrating energy toward a target satellite for improved link gain [4], [5]. Because beam steering is accomplished by electronics, it can be instantaneous, enabling the antenna to rapidly switch or hop between different directions far faster than any mechanical mount. Moreover, phased arrays eliminate moving parts, improving reliability, and reducing maintenance [6].

In communication networks, phased array technology offers capabilities beyond traditional single-beam dishes. One key advantage is the ability to form and steer multiple beams simultaneously from a single array. By using multiple independent sets of phase weights, a phased array can send/receive in several directions at once. He et al. notes that this multi-beam capability is a primary reason phased arrays are considered attractive for future ground stations supporting LEO constellations [6]. In contrast, a mechanical dish is generally limited to one link at a time. Recent technological advances, including compact transmit/receive modules and digital beamforming techniques, now enable dynamic adjustment of beams and nulls even adapting in real time to maximize signal quality. Digital phased arrays can thus track and communicate with many targets, offering unprecedented flexibility.

Despite these advantages, phased arrays come with challenges. A large number of antenna elements are required to achieve high gain and narrow beams – typically hundreds of elements are needed for a gain comparable to a large dish. This can make phased arrays expensive and power-hungry. There are also scan angle limitations: a flat planar array has optimal gain when pointed broadside; steering far off boresight can introduce gain loss and pattern distortion [6]. Various array configurations, such as faceted or conformal arrays, have been proposed to mitigate these issues [6].

Despite challenges, phased arrays are increasingly practical. For example, SpaceX’s Starlink user terminals employ electronically steered arrays to track LEO satellites [2], demonstrating the technology's real-world viability.

2.3 Satellite Tracking Technologies: Phased Arrays vs. Traditional Antennas

Tracking a LEO satellite requires continuously repointing the antenna to follow rapid changes in azimuth and elevation. Historically, this has been achieved with mechanically steered parabolic reflectors, which can offer very high gain but suffer from slow slewing speeds and mechanical wear. Mechanically steered systems typically cannot track multiple satellites simultaneously without deploying multiple antennas, making them impractical for dense LEO constellations.

Phased arrays inherently address these limitations by enabling instantaneous beam steering and multi-satellite tracking [6]. They can create multiple independent beams simultaneously, effectively replacing several dishes with one aperture. In 2019, experimental systems demonstrated phased-array terminals that could track a LEO satellite while simultaneously handing over to a GEO satellite in under a second [3]. Such agility would be difficult or impossible with mechanical systems.

In terms of reliability, phased arrays have no moving parts and therefore promise higher operational uptime and reduced maintenance costs [6]. In contrast, dishes involve motors and gears that are prone to failure, especially under adverse weather conditions. While phased arrays introduce their own complexities, such as the need for calibration of many active electronic elements, the overall reliability tends to be higher.

Performance-wise, phased arrays enable dynamic beam shaping and null steering to optimize signal quality and reduce interference. Traditional dishes have rigid patterns and cannot dynamically adapt. Experimental results, such as those from Adomnitei et al. [7], validate that even small phased arrays can achieve meaningful gain (~12 dBi) for LEO tracking and improve link quality over fixed single-element antennas. As the number of satellites grows, phased arrays are poised to become the dominant technology for ground station tracking systems.

2.4 Research Gaps and Relevance to This Project

Despite the progress in phased array technologies and LEO satellite tracking, gaps remain in the integration and simulation of these systems. Many existing studies either focus on phased array beamforming in isolation or on orbital tracking algorithms without modelling how antenna behaviour affects performance [8], [6].

There is a scarcity of flexible, open simulation frameworks that combine phased array modelling with realistic LEO tracking scenarios.

Earlier works, such as Ng et al. [8], introduced basic MATLAB simulations for phased array tracking, but these efforts were limited by the technology and computational resources available at the time. More recent advances in phased array hardware and the growing complexity of LEO constellations call for updated simulation tools that can handle dynamic multi-beam tracking, performance trade-offs, and system-level optimization.

This project addresses these gaps by developing a modular MATLAB-based simulation framework that dynamically steers beams in response to LEO satellite positions. It combines phased array modelling (computing array factor, beamwidth, steering capabilities) with orbital data (e.g., TLE files) to create realistic dynamic scenarios. This integration enables exploration of key questions such as beam crossover timing, array sizing trade-offs, and tracking precision under multi-target conditions.

By providing a scalable, open simulation tool, this project contributes to understanding and optimizing phased array ground station designs for the next generation of LEO satellite networks. It offers a foundation for future work, including real-time orbit updates, Doppler compensation, and realistic RF link modelling, all of which are critical for operational deployment.

3 Background or System Under Consideration

A flexible simulation framework is essential for phased array satellite system designers to minimize risks associated with the development of multi-beam phased array communication systems. The requirements for such a framework encompass all aspects of analysis, design, implementation, and system lifecycle management. Additionally, these requirements span multiple domains, including both the RF and digital processing aspects of phased array operation. While this increases the complexity of the framework, its value lies in ensuring design requirements are met, optimizing power efficiency, and detecting potential system errors before deployment, ultimately improving overall system performance and reliability.

3.1 Principles and Advantages of Phased Array Antennas

This section draws primarily from established antenna theory texts, including Balanis [4], Mailloux [5], Skolnik [9], and Richards [10], to outline the principles and performance characteristics of antenna arrays relevant to this study.

A single antenna element usually produces a radiation pattern that is wide and offers low directivity or gain. In many communication systems, especially those operating over long distances, antennas must provide higher directivity to ensure efficient signal transmission and reception. One way to increase directivity is by enlarging the size of a single antenna element. However, making individual elements larger is often impractical, particularly when constraints on physical size and weight exist.

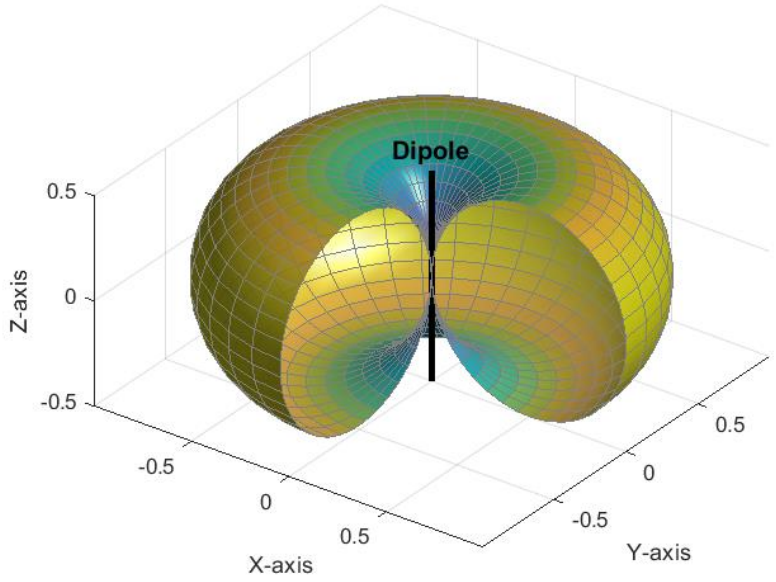

Figure 1 Three-dimensional radiation pattern of a half-wave dipole antenna showing omnidirectional broadside radiation and low directivity.

A single half-wave dipole antenna produces a characteristic doughnut-shaped radiation pattern, with maximum radiation at broadside ($\theta = 90°$) and nulls along the dipole axis ($\theta = 0°$ and $\theta = 180°$). Figure 1 shows this typical pattern, with a cut-out section to better illustrate the inner structure. This pattern highlights the fundamental limitation of a single element in terms of directivity, motivating the use of antenna arrays to achieve more focused beam patterns.

A more effective approach is to combine multiple radiating elements into a structured configuration known as an array. An antenna array increases the electrical size of the antenna system without necessarily increasing the physical size of each element. Typically, arrays are formed using identical elements, although this is not a strict requirement. Elements in an array can take many forms, including wires or apertures, depending on the application.

The radiation pattern of the entire array is determined by the vector addition of the fields produced by the individual elements. This process assumes that each element radiates independently, although in practice, the interaction between closely spaced elements can alter their performance. The primary goal in array design is to ensure that the fields from individual elements add constructively in the desired direction and cancel out in other directions. The array factor (AF), which is a function of both the geometry of the array and the phase excitations of the elements, plays a crucial role in achieving this directive behaviour.

$$AF(\theta) = \sum_{n=0}^{N-1} e^{jn(cos\theta+\beta)}$$

Equation 1 Array Factor for Linear Array

For a uniform linear array, the array factor is given by the equation 1. where N is the number of elements, d is the spacing between elements, k is the wavenumber, and β is the phase shift applied to the elements.

3.1.1 Antenna Plots: Cartesian and Polar

Antenna patterns are often shown using either Cartesian or polar plots. Both methods show the same data, but in a different format. Cartesian plots display the pattern on a graph with gain against angle. This makes it easy to measure beamwidth and compare sidelobe levels. Polar plots show the pattern in a circular format. This gives a better view of how the antenna radiates energy in all directions. It also makes it easier to understand how the antenna behaves in space. Both plot types are common in antenna design. It is useful to understand and use both, depending on what information you need to show.

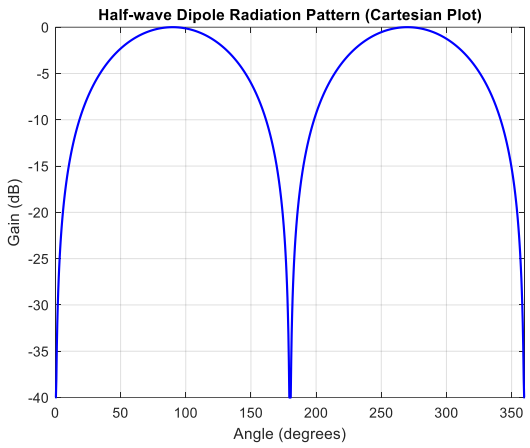

Figure 2 Radiation Pattern (Cartesian Plot) [9]

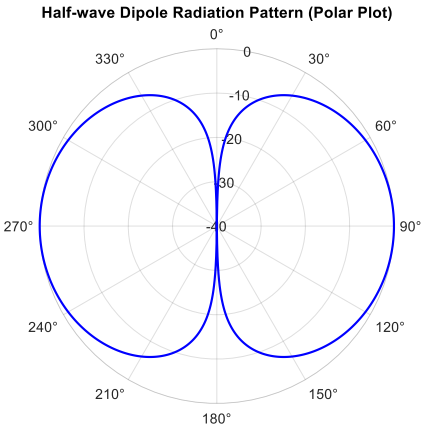

Figure 3 Radiation Pattern (Polar Plot [9])

Two-dimensional radiation pattern of a half-wave dipole antenna shown using both Cartesian and polar plots. The Cartesian plot (left, figure 2) clearly illustrates the broadside radiation and nulls along the axis of the antenna, making it easier to measure beamwidth and sidelobe levels. The polar plot (right, figure 3) presents the same data in a circular format, providing a better visualization of the antenna's omnidirectional radiation characteristics in space.

3.1.2 beamwidth

Beamwidth describes how a transmitting antenna concentrates energy in space. It is one of the most important performance measures in antenna design. A narrow beamwidth means the antenna can focus energy in a specific direction, increasing the signal strength toward a target while reducing power sent in unwanted directions.
In most applications, beamwidth is measured using either the Half-Power Beamwidth (HPBW) or the First Null Beamwidth (FNBW). HPBW is the most common. It is defined as the angular width of the main lobe where the transmitted power drops by 3 dB from its maximum value. FNBW is the angular spacing between the first nulls on either side of the main lobe. [9]

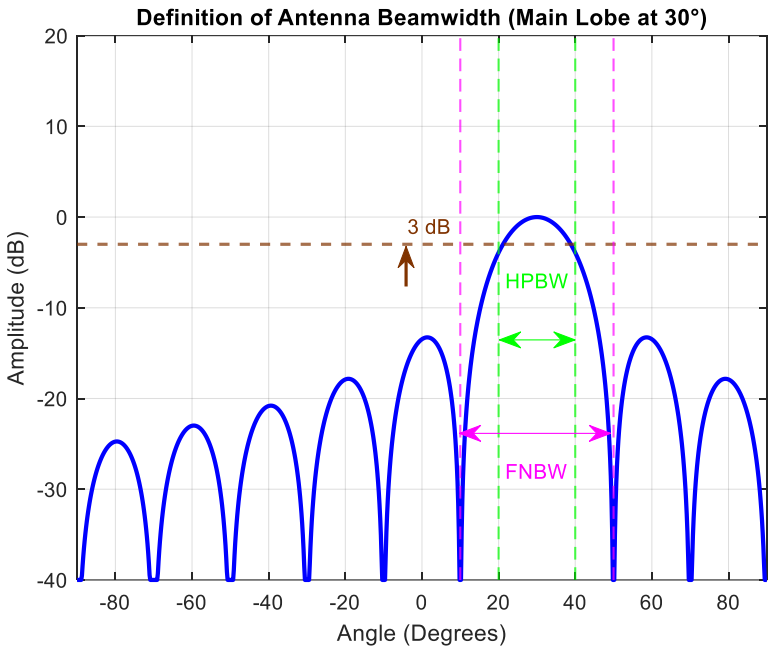

Figure 4 antenna beamwidth (linear array N = 8, d = λ/2, θ = 30°) [9]

Figure 4 shows the definition of beamwidth for a uniform linear array with N = 8 elements, an element spacing of d = λ/2, and a main beam steered to $\theta_0 = 30°$. The HPBW is measured by finding the angular points where the transmitted power falls to half its peak value. This corresponds to a -3 dB drop. The angular distance between these points gives the HPBW.

3.1.3 Beam Steering Phase Shift Equations

Beam steering in an antenna array is achieved by applying incremental phase shifts to each element.

$$\Psi_x = -kd_x m \sin(\theta_s)\cos(\phi_s)$$

Equation 2 X-axis Phase Shift Equation

The X-axis phase shift for element mmm is given in equation 2.

Here, $k = \frac{2\pi}{\lambda}$is the wave number, and d_x is the element spacing along the X-axis. The variable mmm is the element index, θ_s is the steering elevation angle, and ϕ_s is the steering azimuth angle.

$$\Psi_z = -kd_z n \sin(\theta_s)\sin(\phi_s)$$

Equation 3 Z-axis Phase Shift Equation

The Z-axis phase shift for element n is shown in equation 3.
Here, d_z is the spacing in the Z direction, and n is the element index along Z.
Applying these phase shifts aligns the array's main lobe to the direction (θ_s, ϕ_s).

3.2 Beamforming Techniques and Multi-Beam Systems

Beamforming uses many antenna elements. A controller sets each element's phase and amplitude. These signals combine to form a beam in a chosen direction [10]. A phased array has no moving parts and steers beams by electronic phase shifts. This electronic steering is very fast.
In single-beam operation, one set of weights is applied. The array then focuses energy in one direction. In multi-beam systems, additional weight sets are applied. A beamforming network like a Butler matrix can form multiple simultaneous beams, each with full array gain [10]. This allows one array to track many targets at once.
Forming multiple beams raises system complexity and can cause beam overlap. Engineers use adaptive weighting and null steering to reduce interference. Digital beamforming provides full control of the beam shapes [11]. In digital systems, each element's signal is digitized and combined in software. Hybrid analog–digital designs combine both approaches to balance hardware cost and flexibility.

3.3 Simulation Platforms for Antenna System Design

Computer simulation is essential for phased array design. It enables virtual prototyping and reduces the need for physical testing [12]. Simulation reduces development time and cost [12]. Common platforms include MATLAB, CST Studio Suite, and ANSYS HFSS. These tools let engineers test designs in a virtual environment.
MATLAB supports matrix operations, signal processing, and visualization [13]. The Phased Array System Toolbox adds beamforming and array simulation functions [13]. MATLAB code solves many antenna array problems faster than equivalent C or Fortran programs [13]. Researchers often use MATLAB for algorithm development and rapid prototyping of phased arrays.
CST Studio Suite and HFSS are full-wave electromagnetic simulators [12] [14]. These programs solve Maxwell's equations for three-dimensional structures. They compute detailed radiation patterns and element coupling effects. Engineers use these

tools to verify antenna designs and optimize performance. Full-wave simulation can be computationally expensive, so engineers often use it alongside faster system-level models.

3.5 MATLAB Simulation Environment

The phased-array simulations were implemented in MATLAB. A uniform 20×20 planar antenna array was modelled, operating at 76 GHz. Array elements are spaced at half the wavelength (λ/2) to prevent grating lobes and simplify the computations. The software computes the array factor for a given beam direction and visualizes the 3D radiation pattern on a Cartesian grid. Phase shifts are applied to each element to steer the beam electronically. Both single-beam and multi-beam configurations are supported by summing the contributions of different phase profiles. This modular MATLAB framework allows easy adjustment of array size, frequency, and steering angles for further study, consistent with prior MATLAB-based array models [6], [7].

3.6 Phased Array Resolution and performance

In phased array systems, the term resolution denotes the capability of the antenna array to distinguish between two spatially close signals or sources. This property is intrinsically linked to the beamwidth of the array's main lobe. A narrower beamwidth corresponds to a finer angular resolution, which is crucial when tracking multiple satellites or targets within a limited field of view.

$$\theta_{HPBW} \approx \frac{0.886\lambda}{D}$$

Equation 4 HPBW approximation

The angular resolution of a Uniform Rectangular Array (URA) is typically estimated using the half-power beamwidth (HPBW), which can be approximated as shown in equation 4.

where lambda (λ) is the operating wavelength and D is the physical aperture size in the direction of interest. For a planar array, this aperture is determined by the number of elements and their spacing:

$$D_{x} = M \cdot d_x, D_z = N \cdot d_z$$

Equation 5 Array Dimensions

As demonstrated in the developed simulations, resolution was observed to improve with an increase in the number of array elements or a reduction in wavelength, both of

which result in a larger effective aperture. Specifically, higher operating frequencies (e.g., 76 GHz vs. 30 GHz) were found to produce narrower main lobes, enhancing angular discrimination.

However, element spacing was maintained at or below λ/2 to avoid the emergence of grating lobes, which could otherwise compromise the effective resolution and introduce ambiguity in direction finding. The use of uniform spacing and controlled phase shifts facilitated precise beam steering while preserving pattern integrity.

In multi-beam scenarios, the importance of resolution becomes even more evident. Closely spaced beam directions require sufficient angular separation to avoid mutual interference. The simulations confirmed that higher resolution allowed each beam to be resolved distinctly, supporting the system's ability to track multiple LEO satellites simultaneously without significant beam overlap.

These observations are consistent with theoretical models and principles outlined in radar signal processing literature.

3.7 Ethical, Environmental, and Societal Impact

Phased arrays offer many benefits but also raise ethical, environmental, and societal concerns [9]. Dual-use technology is a major ethical issue [10]. Systems designed for civilian use, like satellite tracking, could also support military or surveillance applications [11]. Transparency and adherence to international regulations are essential to address this concern [10]. Ground stations must avoid intercepting unauthorized communications and must respect frequency licensing rules [12].

Environmentally, phased arrays consume significant power, especially when tracking multiple satellites continuously [11]. Designers should prioritize energy-efficient hardware and use adaptive system duty cycling to reduce emissions [9].

Manufacturing arrays also uses rare materials and produces waste [10]. Sustainable sourcing and strong end-of-life recycling strategies should be implemented to reduce environmental harm [12].

Phased arrays can improve global connectivity by enabling internet access for remote regions [4]. However, cost and access barriers must be addressed to avoid deepening the digital divide [9]. Affordable and open technology standards can help ensure that all communities benefit equally [10].

Public engagement is also important for community trust. Communities hosting large antennas must be informed about safety and environmental impacts [11]. Clear

communication about benefits, risks, and protections can prevent opposition to new installations.

Professional ethics codes, such as those by IEEE and IET, must guide engineering decisions [9]. This project aligns with these standards by promoting open, modular simulation tools and responsible technology development [9].

4 Methodology and Research Methods

4.1 Program 1 – Single Beam Steering

Program 1 builds a single directional beam using a 20x20 grid of antenna elements. Each element is spaced half a wavelength apart to avoid grating lobes. The frequency is set at 30 GHz, a common band for LEO satellites. The user specifies a beam direction by entering elevation and azimuth angles.

Input	Description
Frequency (f)	Operating frequency, set to 30 GHz.
Number of Elements (M, N)	20 elements along X and Z axes.
Element Spacing (dx, dz)	Half the wavelength (λ/2) spacing.
Elevation Angle (thetaMax)	Desired elevation beam steering angle.
Azimuth Angle (phiMax)	Desired azimuth beam steering angle.

Table 1 Single Beam Input Table

Inputs needed for the program are shown in table 1.

The program calculates a phase shift for each antenna element based on that target direction. Next, the program computes the array factor by summing signals from all elements. The program uses the signal wavelength and element spacing to compute each element's phase shift. The code applies these phases with MATLAB's complex exponentials (exp(1j * phase)). Then the program sums these values over the 2D grid of elements. The result is the combined field pattern for the given beam direction. Finally, the program plots the radiation pattern in 3D. The plot shows a strong main lobe at the target direction and smaller sidelobes around it. This confirms that phase changes alone can steer the beam without moving parts.

4.1.1 1D Array Factor Summations (X and Z directions)

Using the steering phases from Chapter 3, the array factor in each direction is computed by summation.

For the X-axis, the array factor is the sum of contributions from all elements:

$$AF_X = (\theta, \phi) = \sum_{m=0}^{M-1} e^{j[kd_x m \sin(\theta)\cos(\phi)+\Psi_x(m)]}$$

Equation 6 X-axis 1D Array Factor Equation

Here, AF_X is the X-axis array factor, and M is the total number of elements in the X direction. The term $\Psi_x(m)$is the steering phase from Equation 6.

$$AF_Z = (\theta, \phi) = \sum_{n=0}^{N-1} e^{j[kd_z n \sin(\theta)\sin(\phi)+\Psi_z(n)]}$$

Equation 7 Z-axis 1D Array Factor Equation

Here, AF_Z is the Z-axis array factor, and N is the total number of elements in the Z direction. The term $\Psi_z(n)$is the steering phase from Equation 7.
These summations compute the radiated field components from each axis independently before combining them into the full array pattern.

4.1.2 2D Array Factor Product for Full Planar Array

For the full planar array, the total array factor is obtained by multiplying the X and Z factors. This leverages the fact that the axes are independent.

$$AF(\theta, \phi) = AF_X(\theta, \phi) \times AFF_Z(\theta, \phi)$$

Equation 8 Full 2D Array Factor Equation

The total array factor is given the equation shown in equation 8.
Here, AF is the overall array factor, and AF_X and AF_Z are the factors from Equations (4.1) and (4.2). The product $AF_X * AF_Z$ yields the combined radiation pattern of the 2D array.

4.2 Program 2 – Multi-Beam Steering

Program 2 extends the single-beam design to form multiple beams at once. It uses the same 20x20 grid of antenna elements and element spacing as before. The user enters a list of elevation and azimuth angles, one pair for each desired beam.

Input	Description
Frequency (f)	Operating frequency, set to 30 GHz.
Number of Elements (M, N)	20 elements along X and Z axes.
Element Spacing (dx, dz)	Half the wavelength (λ/2) spacing.
Number of Beams (numBeams)	User-specified number of beams.
Elevation Angles (thetaMaxArray)	Elevation angles for each beam.

Azimuth Angles (phiMaxArray)	Azimuth angles for each beam

Table 2 Multi Beam Input Table

The inputs

The program uses these angles as inputs for the beam calculations. For each beam, it computes an array factor using the same method as in Program 1.

Next, the program calculates the total array factor by summing the contributions of each beam. It computes each beam's signal pattern separately using the phase shifts for that beam's direction. Then the program adds those patterns elementwise in MATLAB. This uses the principle of superposition of waves. The final result is a combined 3D pattern with multiple main lobes. The program plots this combined pattern to show all beams.

4.2.1 Multi-Beam Superposition Method

In the multi-beam scenario, each beam's array factor is computed separately and then summed. The fields add linearly to produce multiple lobes.

$$AF_{total}(\theta, \phi) = \sum_{b=1}^{B} AF_b(\theta, \phi)$$

Equation 9 Multi-Beam Superposition Equation

The combined array factor for B beams is shown in equation 9.

Here, B is the number of beams and AF_b is the array factor of beam b with its own steering angles. Summing these factors creates a multi-lobe pattern, with each lobe corresponding to one of the steering directions.

4.3 Role of beam Simulations in Final Project

The single-beam and multi-beam programs form the foundation of the simulation framework. They show that a phased array can steer signals electronically by adjusting the phases at each element. Users can verify the array factor calculations by checking the output beam directions and shapes. The output radiation patterns provide visual confirmation that the steering logic works. These core modules handle the basic tasks of creating and combining beams from the antenna array.

These programs focus on beam steering logic and do not include satellite orbit tracking or signal-to-noise ratio (SNR) calculations. They use ideal conditions and fixed parameters for testing. The output pattern shows how the main beam and

sidelobes move with different input angles. These results help validate the array design and beamforming method. Overall, the simulation code provides a working proof of concept for phased array steering.

4.4 Orbit Prediction and the Role of TLE Data

Orbit prediction is a key part of tracking satellites. This project uses Two-Line Element (TLE) files to predict satellite paths across the sky. A TLE file contains simple orbital data that ground stations can use without heavy computing. The TLE data used in this project was obtained from CelesTrak [21], a trusted online source for real-time satellite tracking information (all data used in appendix F).
Each TLE entry has three lines.

```
COSMOS 2361
1 25590U 98076A   25085.24608917  .00000132  00000+0  12624-3 0  9991
2 25590  82.9383 177.4391 0030059 272.7097 145.0986 13.73184118315525
```

Figure 5 TLE COSMOS example.

The first line shows the satellite name, making it easy to identify. The next two lines hold the real orbital data, broken into smaller fields. These fields describe the shape, tilt, and speed of the orbit in space.

Field	Meaning
Line Number (1)	Identifies this as the first data line
Satellite Number (25590)	Unique satellite ID assigned by NORAD
Classification (U)	U = Unclassified, C = Classified
Launch Year and Launch Number (98076A)	98 = 1998 launch year, 076 = 76th launch, A = first piece
Epoch (25085.24608917)	85th day of 2025, fractional day
First Derivative of Mean Motion (0.00000132)	Rate of change of mean motion (rev/day²)
Second Derivative of Mean Motion (00000+0)	Often zero; rarely used unless under special conditions
BSTAR Drag Term (12624-3)	Atmospheric drag parameter
Ephemeris Type (0)	0 = Standard SGP4 model
Element Set Number (999)	Version number for updates
Checksum (1)	Error-checking number

Table 3 TLE line 1 field breakdown

Table 3 shows an example of a TLE file. Each field is labelled to help the reader understand what the numbers mean. Knowing how to read a TLE is important for any satellite tracking system.

Field	Meaning
Line Number (2)	Identifies this as the second data line
Satellite Number (25590)	Repeats satellite ID for verification
Inclination (82.9383°)	Angle between orbit plane and Earth's equator
Right Ascension of Ascending Node (177.4391°)	Longitude where the orbit crosses the equator going north
Eccentricity (0.0030059)	Shape of orbit (0 = circular, near 0 = low eccentricity)
Argument of Perigee (272.7097°)	Angle to the orbit's closest approach to Earth
Mean Anomaly (145.0986°)	Position of satellite in orbit at the epoch
Mean Motion (13.73184118 rev/day)	Number of orbits the satellite makes per day
Revolution Number at Epoch (31552)	Total orbits completed at epoch time

Table 4 TLE line 2 field breakdown

Not every value inside a TLE file is needed for this project. Only certain fields are used to predict the satellite's path and motion. Table 4 lists the fields chosen and the parts of the orbit they control.

For example, inclination tells how much the orbit tilts from the Earth's equator. Mean anomaly tells where the satellite is along its path at a given time. Mean motion shows how fast the satellite travels around the Earth.

Table 3 explains why each field was important for this project. Each field links to a real need during orbit building, such as setting the orbit's shape or speed. Choosing the right fields keeps the system efficient and easy to simulate.

Using TLE files allows quick orbit prediction with simple tools. This choice supports early-stage antenna design and planning. It also makes the system flexible for education and low-cost ground station projects.

4.5 SNR Calculation and Application

This project includes SNR calculation as a critical part of beam evaluation. SNR measures how strong the received signal is compared to the background noise. A higher SNR value means a better-quality communication link.

$$P_r = P_t G_t G_r (\frac{\lambda}{4\pi d})^2$$

Equation 10 Friis transmission

The simulation calculates received signal power using the Friis transmission equation shown in equation 10. The terms in the Friis equation are defined as follows. Pr is the received power at the ground station. Pt is the transmitted power from the satellite. Gt and Gr are the gains of the transmitter and receiver antennas. λ is the wavelength of the transmitted signal. d is the distance between the satellite and the ground station.

The simulation assumes free-space loss only. Atmospheric loss, fading, or Doppler effects are not included. Noise power P_N is modelled as a constant system noise floor.

$$SNR = \frac{P_r}{P_N}$$

Equation 11 signal-to-noise ratio Equation

The signal-to-noise ratio is calculated by equation 11. SNR values are computed for each beam in every simulation step. These values determine which satellites to track and help optimize beam directions.

4.6 Simulation Workflow Summary

The simulation runs a complete tracking and beamforming process in MATLAB. Satellite orbit data and array settings feed into steering and signal calculations. Each time step uses new satellite positions and signal metrics to adjust the beams. The system updates beams based on signal-to-noise ratio (SNR) and the array's resolution limits.

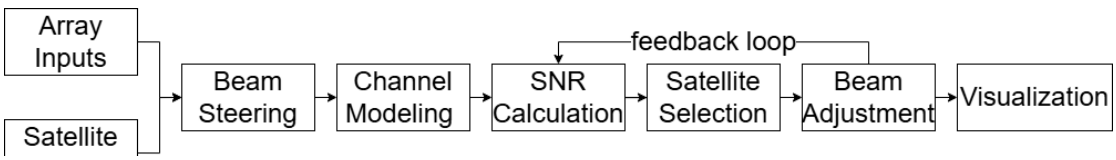

Figure 6 Simulation Flow Diagram

4.6.1 Simulation Inputs

The user sets the antenna array parameters and selects a set of satellites to track. Inputs include the number of elements (e.g. 20×20), element spacing, and operating frequency. The program also reads satellite Two-Line Element (TLE) data for each target. TLE files list orbital parameters of the satellites. This data format encodes each satellite's orbit and motion.

A function (readTLEfile) extracts satellite names and TLE lines from the file. The function groups lines into 3-line blocks for each satellite and returns arrays of line data. Another step processes these lines into 3D position vectors using a simple orbital model. The simulation assumes fixed time steps (e.g. 360) to track satellite movement over time.

4.6.2 Orbit Prediction and Beam Angles

The simulation computes each satellite's location in 3D space. Using the TLE data, the code finds satellite coordinates in an Earth-Centered Inertial (ECI) frame. The program then converts these coordinates to azimuth and elevation angles as seen from the ground station. Any satellite below the local horizon is ignored. These angles show where in the sky each satellite is at the current time step.

4.6.3 Beamforming and Channel Model

Based on the satellite angles, the simulation calculates phase shifts for each antenna element. Phase shifts steer each beam toward the desired azimuth and elevation. For each beam, the simulation computes an array factor by summing the contributions of all elements with their phase delays.

Next, the simulation applies a channel model to compute signal strength. It uses a free-space loss model. In free space, signal power falls off with distance squared. The model uses the satellite distance (from orbit data) and frequency to calculate received power. The antenna gains are included, assuming ideal elements. The received signal power is compared to a noise level to find SNR (signal power divided by noise power).

4.6.4 SNR Feedback Loop

The calculated SNR for each beam link feeds back into the steering logic. The program uses the SNR results to adjust the beams. This improves link quality. For example, if one beam has low SNR, the code might shift that beam or swap to another satellite. This creates a feedback loop. After each calculation, the beam directions

update based on the new SNR. This loop runs every time step, letting the array adapt to changing satellite positions and signal levels.

4.6.5 Satellite Selection and Beam Adjustment

The simulation picks the satellites with the highest SNR values. Typically, up to three satellites are tracked with separate beams. Each chosen satellite gets a dedicated beam steered toward its angle. The code enforces a steering resolution: beam angles are snapped to the nearest allowable step. If snapping causes misalignment, the simulation applies a gain correction using a sinc-based formula. This adjusts the SNR to account for any signal loss. These corrections yield final beams that best track the chosen satellites.

4.6.6 Visualization

The simulation provides real-time plots to show results. One plot is a 3D view of the antenna's active beam patterns. This plot updates each time step with the current beam directions and strengths. Another plot shows satellite orbits and the ground station. The plot marks the current position of each tracked satellite on its orbit path in real time. These visuals make it easy to see which satellites are tracked and how the beams point in space.

4.6.7 Conclusion

This workflow ties together array inputs and satellite data in a loop of beam steering and signal evaluation. The system starts with configuration and TLE orbit data. The simulation calculates where each satellite is and where to point each beam. The code then computes the signal path and finds the SNR, using that feedback to adjust the beams. This process repeats at every time step. Finally, the simulation selects the best satellites and adjusts the beams for them. The results are shown visually.

5 Simulations, Testing and Evaluation

5.1 Spherical to Cartesian Coordinate Transformation for Plotting

Visualization of the radiation pattern requires converting spherical coordinates to Cartesian coordinates. Each point on the pattern has spherical coordinates (R, θ, ϕ), where R is the magnitude (radius) at angle (θ, ϕ). The conversion equations are:

$$x = Rsin(\theta)cos(\phi)$$

Equation 12 x-Coordinate Transformation Equation

$$y = Rsin(\theta)\sin(\phi)$$

Equation 13 y-Coordinate Transformation Equation

$$z = Rcos(\theta)$$

Equation 14 z-Coordinate Transformation Equation

Here, x, y, and z are the Cartesian coordinates of the point shown in equation 12,13,14 in order. The variable R is the value of the radiation intensity or field magnitude at that point. The angle θ is the elevation from the positive Z-axis, and ϕ is the azimuth around the Z-axis. Using these equations maps the spherical beam pattern into a 3D Cartesian space for plotting.

5.1 Single Beam Steering Test

The single beam steering test focused on verifying that the phased array could correctly direct energy toward different azimuth and elevation angles. Simulations were run with varying steering commands and array configurations to observe changes in the radiation pattern. Performance was evaluated based on beam direction accuracy, beamwidth, and sidelobe behaviour (code used in appendix C).

5.1.1 steering angle testing

In this test, the array configuration was fixed at 20 × 20 elements with λ/2 element spacing, operating at 30 GHz. The goal was to observe how changing the desired azimuth (ϕ) and elevation (θ) angles affects the radiation pattern.

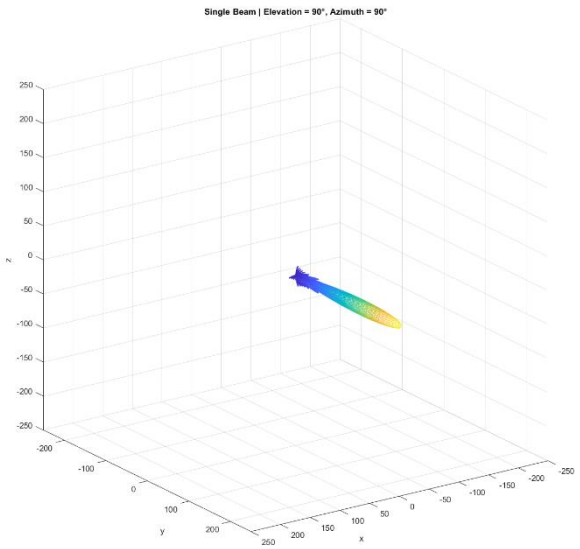

Figure 7 Single Beam | Elevation = 90°, Azimuth = 90°

Test 1 (90°/90°): Beam pointed directly upward from the array surface as shown in figure 7. Main lobe very symmetrical, minimal distortion. Beamwidth was narrowest because steering is cantered along the array normal (boresight).

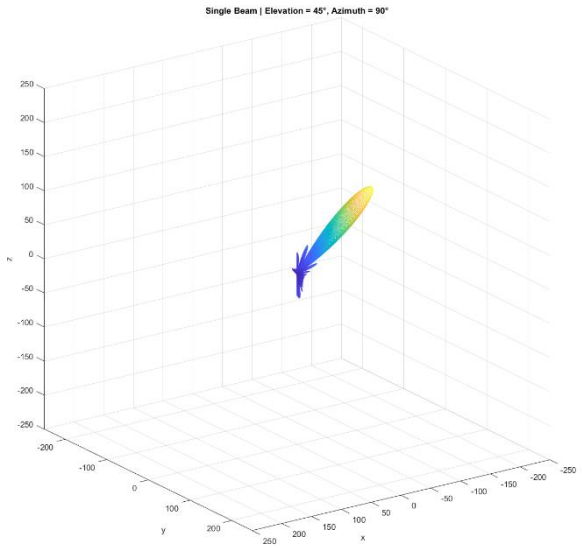

Figure 9 Single Beam | Elevation = 90°, Azimuth = 45°

Test 2 (90°/45°): Beam tilted toward the horizon at a medium elevation as shown in figure 9. Main lobe slightly wider compared to boresight.

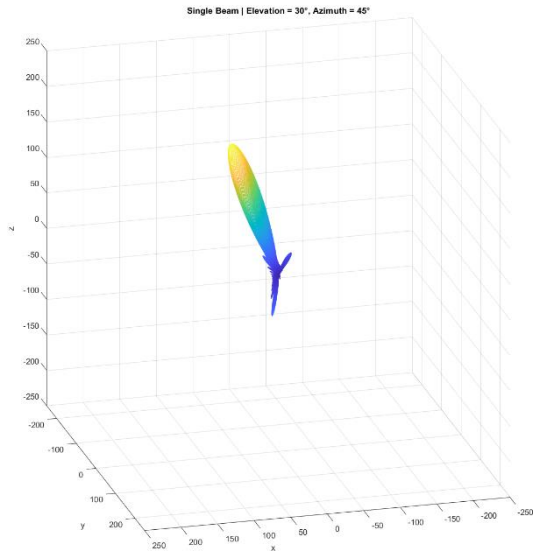

Figure 8 Single Beam | Elevation = 45°, Azimuth = 30°

Test 3 (45°/30°): Beam steered diagonally off the X- and Z-axes as shown in figure 8. Minor beam distortion observed as expected due to off-axis steering. (‘view(145, 20)’ changed to ‘view(165, 20)’ for a clearer view angle)

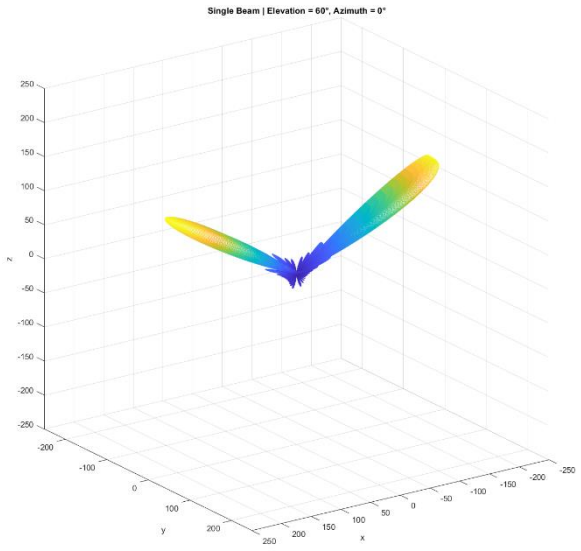

Figure 10 Single Beam | Elevation = 0°, Azimuth = 60°

Test 4 (0°/60°):

Beam tilted toward 0° azimuth at medium elevation as shown in figure 10.

Two symmetric beams were observed in opposite directions (0° and 180° azimuth).

This occurred because the phase steering uses a cosine function, which is symmetric about 0°, causing equal beam formation forward and backward.

5.1.2 Array Size testing

This test studied how changing the number of array elements affects the beamwidth, directivity, and peak array factor magnitude. The element spacing and operating frequency were kept constant, while the array size was varied. The purpose was to confirm that larger arrays produce narrower beams and higher peak intensity.

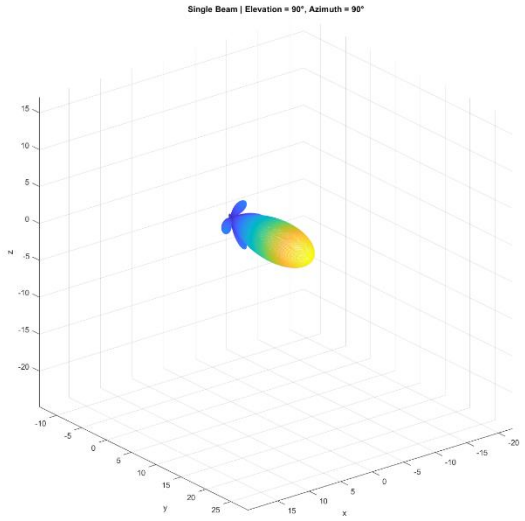

Figure 11 Single Beam | 4 x 4 elements

Test 1 (4 × 4 elements):

The beam was extremely wide and poorly focused as shown in figure 11.

The main lobe covered a broad angular region, and peak gain was very low.

Radiation resembled an almost omnidirectional pattern, with very little beam shaping.

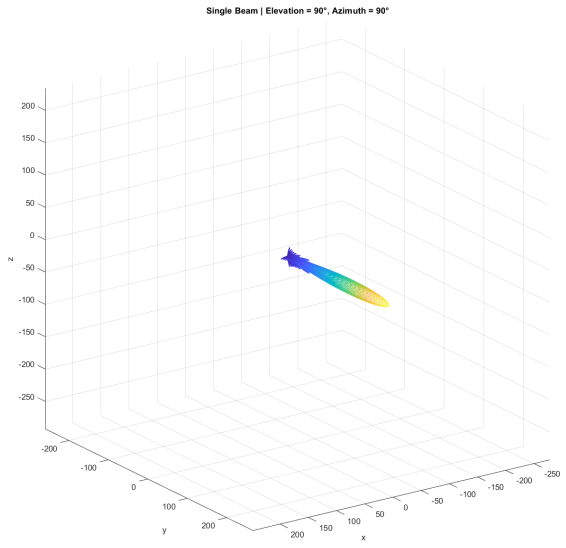

Figure 12 Single Beam | 16 x 16 elements

Test 2 (16 × 16 elements):

The beam became more focused compared to 4 × 4 as shown in figure 12, but still relatively broad. Peak gain improved, and sidelobe structure started to become visible.

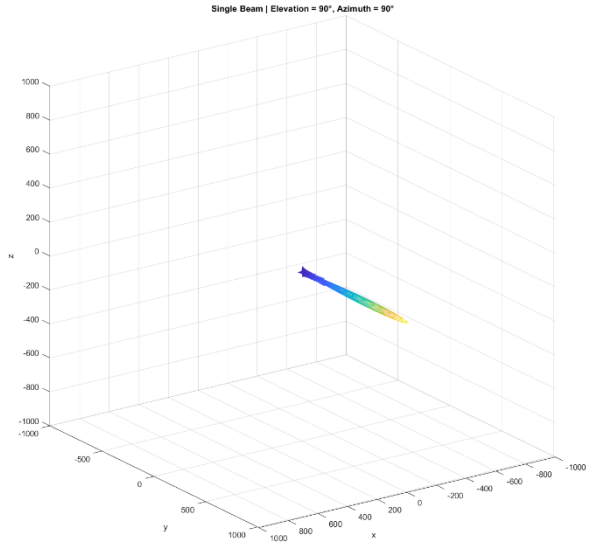

Figure 14 Single Beam | 32 x 32 elements

Test 3 (32 × 32 elements):

A narrower and better-formed beam was observed as shown in figure 14.

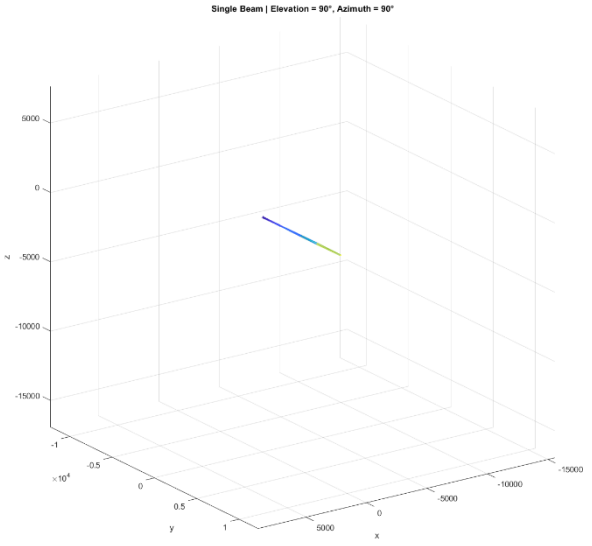

Figure 13 Single Beam | 100 x 100 elements

Peak gain increased, and sidelobes became sharper and more organized as shown in figure 13.

Test 4 (100 × 100 elements):

The narrowest and most highly focused beam was produced.

Peak gain was highest, and sidelobes became extremely thin, although slightly higher in relative level.

The results confirm that beamwidth is inversely proportional to the array aperture size, following the relation $\theta_{BW} \approx \frac{70\lambda}{D}$ where D is the effective array dimension. Larger arrays concentrate energy into smaller angular regions, improving tracking precision.

5.1.3 Gain Drop-off with Steering Angle Test

As the steering angle moves further from boresight, the effective aperture becomes smaller. A smaller aperture causes a drop in the array's gain. Phased array antennas achieve maximum gain when the beam points straight out from the array plane.
At large steering angles, phase errors start to build across the elements. These errors distort the shape of the main lobe. Grating lobes can also appear and pull energy away from the main beam.

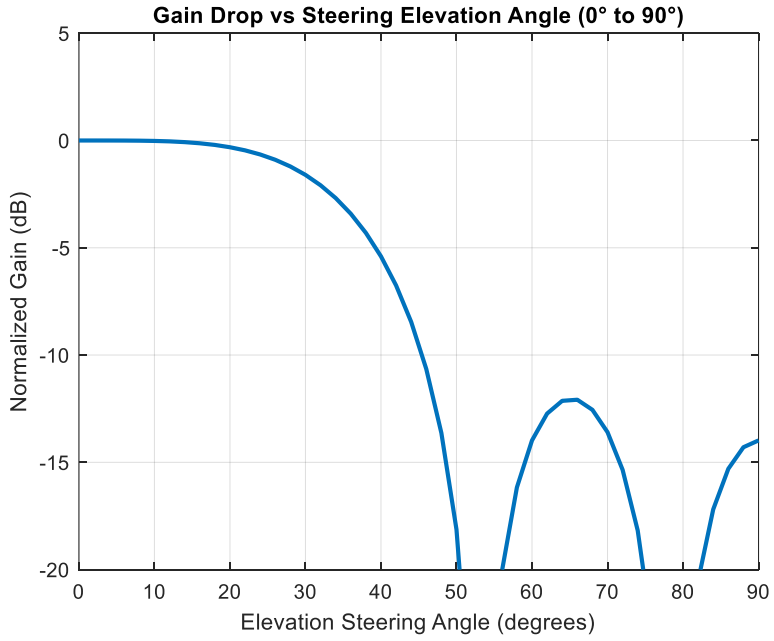

Figure 15 Normalized gain vs steering elevation angle showing reduction in array performance as the beam is steered away from boresight

Both effects cause additional loss of gain and beam quality as shown in figure 15. The array performs best when steering within a small angle from boresight. This behaviour matches the basic theory behind phased array antennas.

5.1.4 grating Lobe testing

Arrays must have element spacing smaller than or equal to half a wavelength (λ/2) to avoid grating lobes. Grating lobes occur when the array spacing allows multiple angles to satisfy the beamforming condition. These secondary beams pull energy

away from the main lobe, lowering effective gain. As steering angle increases, grating lobes become stronger and dominate at wide angles.

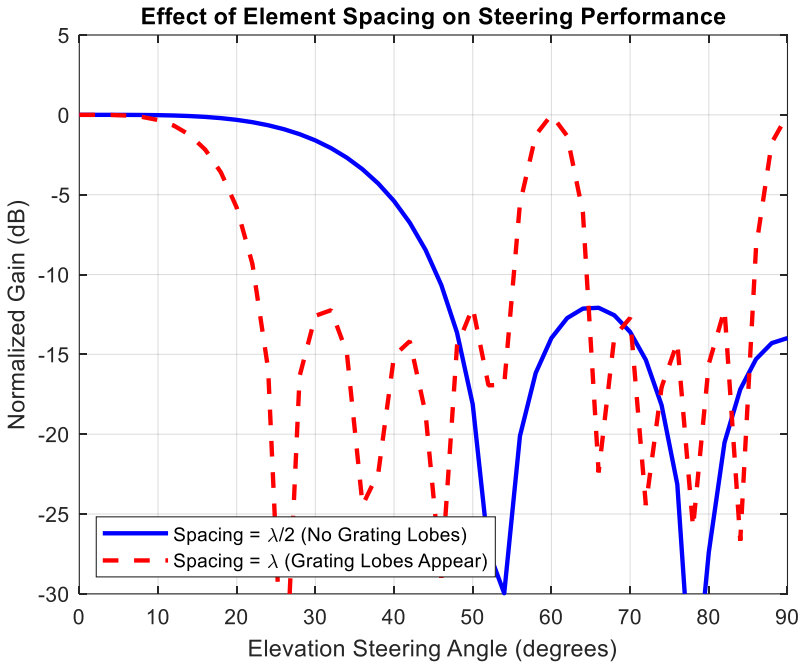

Figure 16 Grating lobes began to appear when element spacing exceeded half-wavelength, especially at large scan angles.

The simulation results in figure 16 showed that arrays with λ/2 spacing scanned smoothly, while arrays with λ spacing exhibited visible grating lobes above 30° steering. This behaviour matches basic array antenna theory.

5.1.5 Array Resolution and Beamwidth Testing

Phased array antennas achieve narrower beams by using more elements across the array aperture. A larger number of elements results in a smaller beamwidth, improving tracking accuracy. However, beamwidth increases when the beam steers away from broadside due to aperture foreshortening.

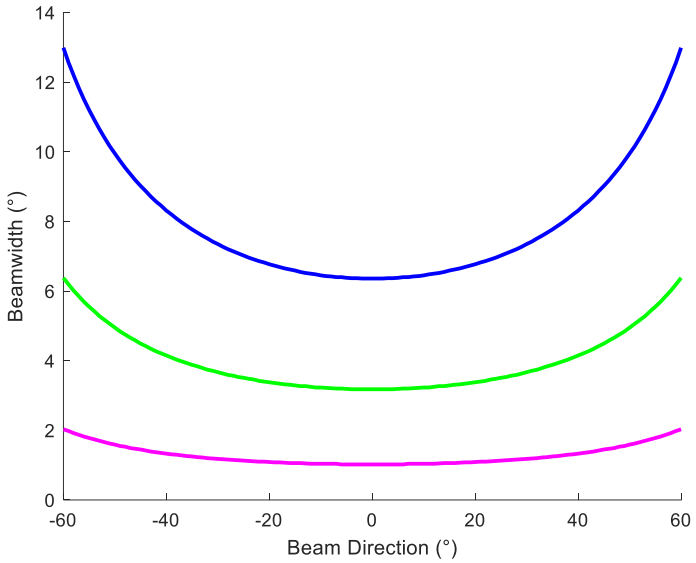

Figure 17 Beamwidth vs Steering Angle for Arrays with 16, 32, and 100 Elements [9]

(The blue curve represents the array with 16 elements, the green curve represents the array with 32 elements, and the pink curve represents the array with 100 elements.)
The simulation results in figure 17 showed that arrays with 100 elements had a beamwidth of around 1° near boresight. Arrays with 32 and 16 elements showed wider beams of about 3° and 6°, respectively. Beamwidth approximately doubled at steering angles beyond 60°, following the expected cos(θ) behaviour.
This result matches basic phased array theory. Narrower beams require more elements. Wide-angle steering reduces array resolution and tracking precision.

5.2 Multi-Beam Steering Test

The second simulation introduced multiple beam directions. The user was prompted to enter several azimuth and elevation angles to simulate multiple satellite targets. The

program computed the superimposed array factors and produced a composite 3D pattern. Tests included up to four beam directions simultaneously, and the simulation successfully resolved each beam in its respective direction, demonstrating the system's capacity for multi-satellite tracking.

5.2.1 steering angle testing

This test series investigates the performance of the array when forming multiple beams. Beam directions were entered manually in MATLAB using the beam pattern simulation script. All beams were kept between 30° and 150° (in both azimuth and elevation) unless otherwise noted, to avoid confusion caused by back lobes (code used in appendix D).

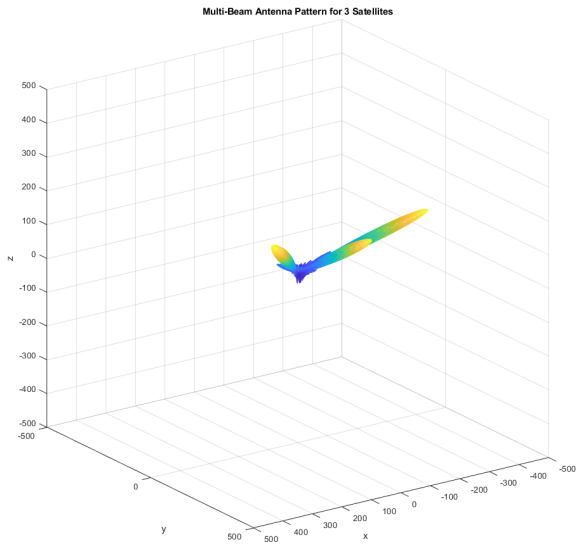

Figure 18 MultiBeam Steering Angle Test 1

Test 1: Wide Beam Separation

Input: 3 beams at φ = 0°, 60°, and 120° / θ = 45° for all as shown in figure 18

Purpose: To observe clear separation between beams

Observation: Beams form in distinct directions with minimal overlap

Conclusion: Array resolves wide angles effectively; superposition is clean

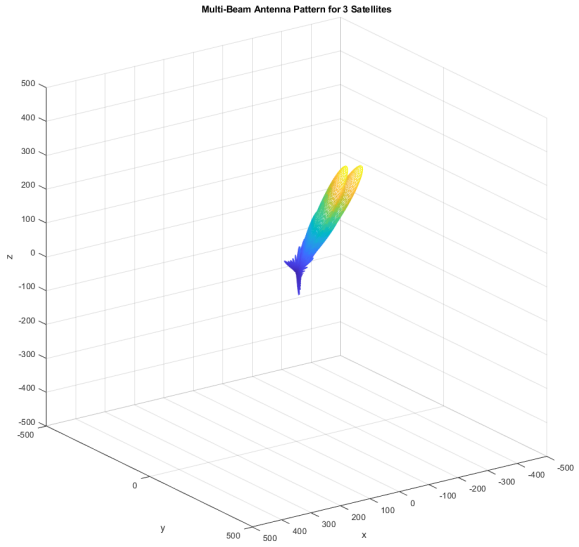

Figure 19 MultiBeam Steering Angle Test 2

Test 2: Closely Spaced Beams

Input: φ = 70°, 75°, 80° with θ = 45° as shown in figure 19.

Purpose: Test array resolution for beams close in angle

Observation: Peaks were slightly merged; visible side lobes increased

Conclusion: Resolution is limited; spacing must be sufficient to avoid pattern distortion

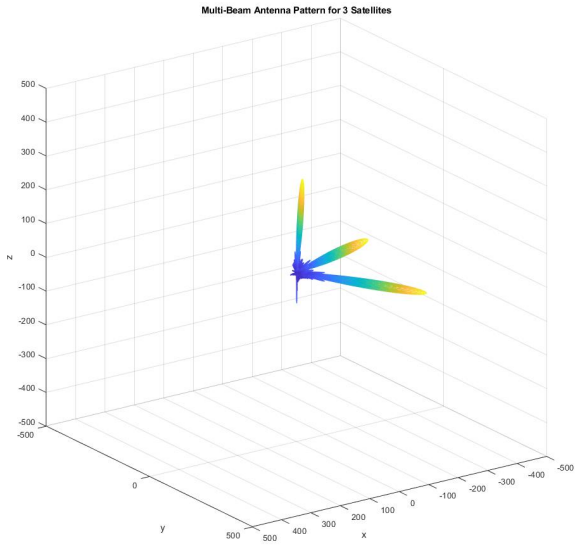

Figure 20 MultiBeam Steering Angle Test 3

Test 3: Unequal Elevation

Input: φ = 60°, 90°, 120° with θ = 30°, 60°, 90° as shown in figure 20.

Purpose: Evaluate beam control over elevation

Observation: Beams were clearly formed at different heights

Conclusion: Array correctly handled elevation steering alongside azimuth

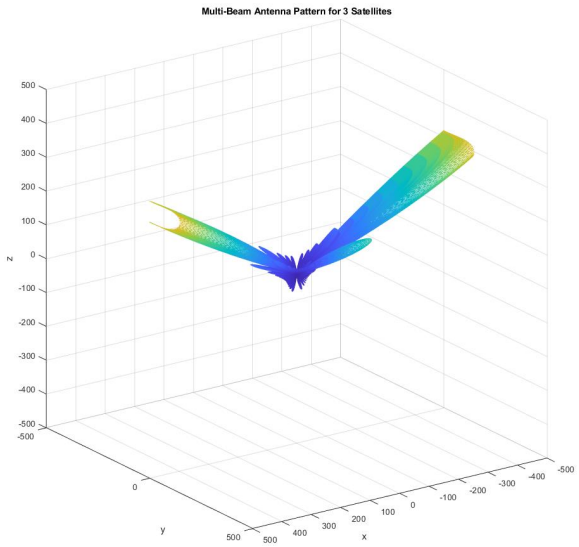

Figure 21 MultiBeam Steering Angle Test 4

Test 4: Edge Case with Back Lobe Effect

Input: φ = 10°, 90°, 170° with θ = 60° as shown in figure 21.

Purpose: Intentionally steer one beam near the edge of the array's angular range

Observation: The φ = 10° beam produced a strong back lobe near φ = 170°, which overlapped with the front lobe of the 170° beam. This caused both beams to combine and form a single, much stronger lobe.

Conclusion: When beams are placed at opposite edges, overlapping lobes can interfere constructively, producing misleading results. Steering near 0° or 180° should be avoided unless specifically required.

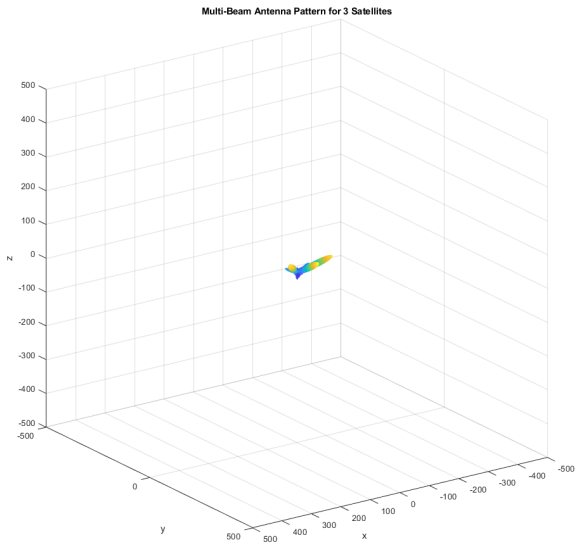

Figure 22 MultiBeam Steering Angle Test 5

Test 5: Smaller Array Size (10×10) vs. Standard (20×20)

Input: φ = 45°, 90°, 135° with θ = 60°, using a 10×10 array as shown in figure 22

Observation: Beams appeared slightly wider compared to the standard array, and visually shorter due to reduced gain. Despite this, the beam directions and spacing remained consistent with the 20×20 case.

Conclusion: For widely spaced beams, a smaller array still forms distinct lobes. However, total gain is lower, and a larger array offers better control in close-beam scenarios or when higher resolution and stronger signal focus are needed.

5.2.2 Number of beams testing

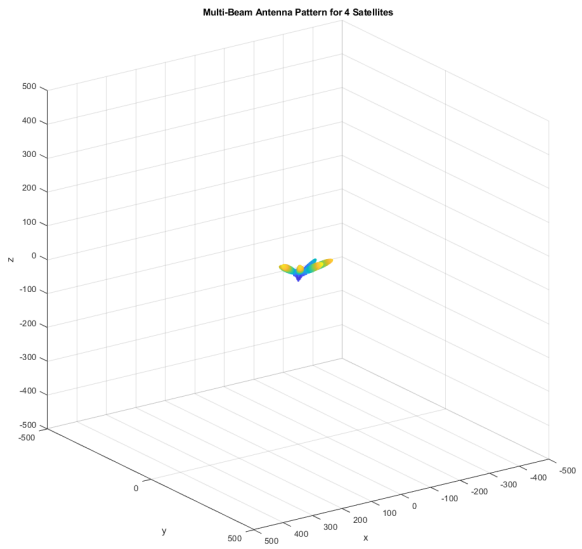

Figure 23 Multibeam 4 Beam Test 1

Test 1: Four Beams – High Utilization Scenario

Input: φ = 30°, 60°, 90°, 120° with θ = 60°, using a 20×20 array as shown in figure 23

Purpose: Evaluate array performance when tracking four simultaneous beams across a wide angular spread

Observation: All four beams were distinguishable, though some minor side lobe overlap was visible. Main lobes remained defined, with reduced gain per beam due to energy division.

Conclusion: The array handles four beams effectively when spacing is sufficient. Beam width increases slightly, but tracking remains stable and clear.

Test 2: Five Beams – Approaching Array Limit

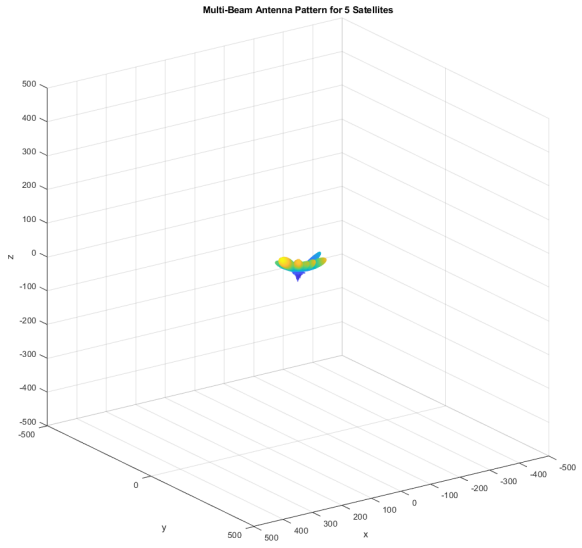

Figure 24 Multibeam 5 Beam Test 2

Input: φ = 30°, 45°, 60°, 75°, 90° with θ = 60°, using the same 20×20 array as shown in figure 24

Purpose: Stress test the system by increasing beam density

Observation: Beams began to interfere with one another. Side lobes overlapped, and some main lobes merged visually. Beam clarity and directionality declined beyond four beams.

Conclusion: Five closely spaced beams push the resolution limits of the 20×20 array. For reliable separation, either increased angular spacing or a larger array would be required.

5.3 SNR Tracking Test of Starlink Satellites

The simulation tested the system by tracking five Starlink satellites using three beams. Each beam selected the satellite offering the highest SNR at each time step. The simulation calculated SNR values based on satellite distance, array gain, and free-space loss.

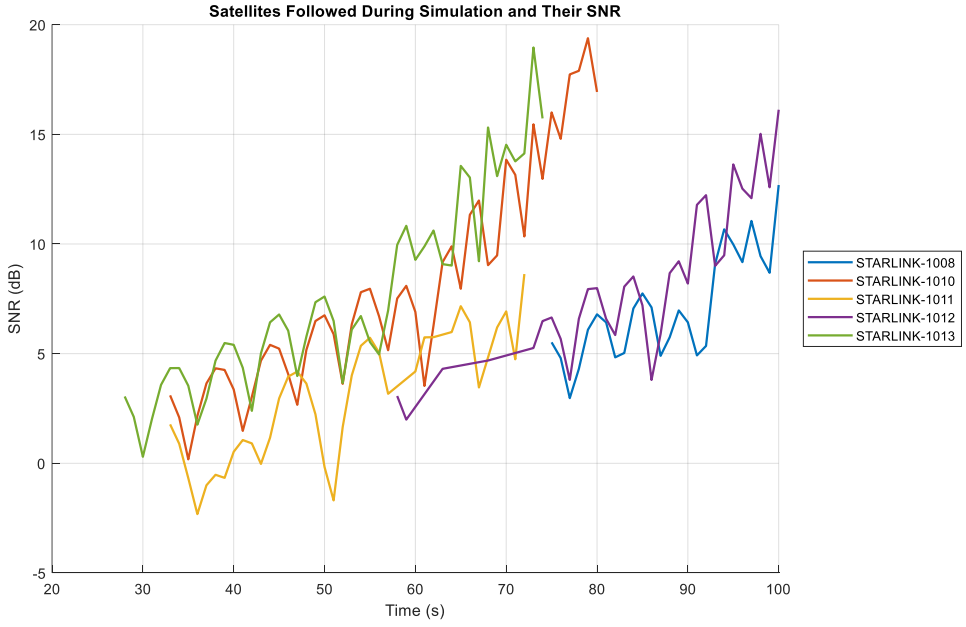

Figure 25 signal-to-noise ratio graphed from example simulation

Figure 25 shows the SNR for all tracked satellites over the simulation time. Satellites STARLINK-1010 and STARLINK-1013 achieved the highest SNR values. These satellites showed steady improvement in SNR, reaching peaks above 15 dB. In contrast, STARLINK-1011 dropped to lower SNR values and became a less favorable target.

The overall SNR trends increase as satellites move closer to the ground station and approach boresight. Small rapid changes in SNR are caused by the beam steering resolution. Since the beam can only snap to discrete angles, slight offsets from the exact satellite position create small SNR fluctuations.

The results demonstrate dynamic beam switching based on signal strength. Beams preferred satellites with rising SNR and dropped satellites with falling link quality. This confirms the adaptive steering logic and shows successful tracking of the best available satellites. More simulations can be found in the GitHub project by scanning the QR code in appendix A.

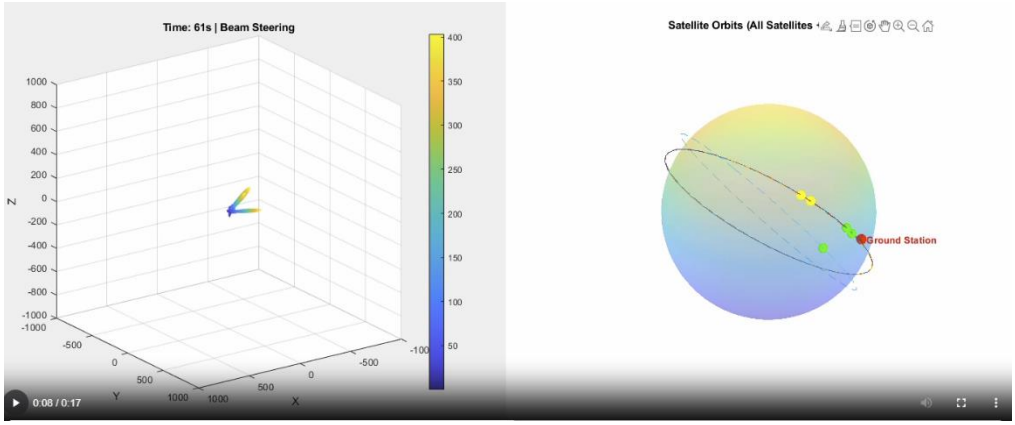

Figure 26 screen shot of the simulation video (same simulation that made figure 17)

Figure 26 shows a screen capture from the simulation video linked to Figure 25. The video shows real-time tracking of LEO satellites. Beam directions adjust automatically based on the strongest SNR. The screen capture confirms the model's ability to track multiple satellites as they move.

5.3 Parameter Variation and Performance Evaluation

Further testing involved modifying key parameters such as:

Array size (M x N): Increasing the number of elements resulted in narrower beams and higher gain.

Element spacing: Adjusting the spacing showed the expected impact on grating lobes, especially beyond λ/2.

Frequency: Simulations at 30 GHz and 76 GHz demonstrated the effect of wavelength on directivity and beam shape.

Each test was accompanied by a 3D mesh plot to visualize beam directions and intensity, providing a valuable tool for debugging and system validation.

6 Results, Analysis and Discussion

6.1 Results

The simulation generated clear far-field beam patterns for single-beam and multi-beam cases. Single-beam steering was accurate and stable over the full scan range. The main lobe pointed correctly at each target angle. Multi-beam operation produced distinct lobes for each satellite, showing that energy could be directed to multiple targets simultaneously. With more antenna elements or higher frequency, each main beam became narrower, matching theoretical [22]. For example, larger arrays achieved finer spatial resolution. In multi-beam tests, separate beams showed minimal overlap when satellites were well-separated. Slight interference appeared when two beams overlapped in angle. Overall, beam shapes behaved as the uniform array model predicts.

The simulation also tracked LEO satellites using live orbital data and SNR calculations. At each time step, the code computed the SNR for all visible satellites. It then allocated beams to the three satellites with the highest SNR values. Each chosen beam was steered toward its satellite's azimuth and elevation. Over time, beams adjusted as satellites moved across the sky. If a satellite's SNR dropped below another's, the code switched the beam to the stronger signal. This dynamic selection kept the tracked links at high SNR and demonstrated the model's ability to maintain signal quality. Across trials, the selected satellites had noticeably higher SNR than the non-tracked ones, indicating effective link prioritization.

The simulation recorded quantitative outputs of SNR and qualitative beam patterns. In one scenario, tracked satellites maintained SNR levels around the chosen threshold despite orbital motion. Beam switching events were visible when satellites moved in and out of the array's field of view. The model did not output detailed metrics like half-power beamwidth or sidelobe levels, but the plots suggest these followed theory. For instance, patterns showed well-defined -3 dB points. Grating lobes only appeared if element spacing exceeded half a wavelength. No unexpected distortions or instabilities were observed in the time-domain results. In summary, the results

objectively show that the phased array steered correctly and the SNR-based tracking selected and maintained the strongest satellite signals.

6.2 Analysis and Discussion

The results confirm that an electronically steered phased array can reliably track satellites with multiple beams [22]. Steering accuracy remained high and repeatable. As theory predicts, adding elements to the array narrowed each beam's half-power width [22]. This was evident in the simulation when comparing small and large arrays. The theoretical half-power beamwidth (HPBW) was effectively the angle between points 3 dB below the peak [22]. In practice, the simulation showed that a larger array achieved finer pointing accuracy. However, steering off boresight incurred trade-offs: the main beam's gain fell and sidelobe levels rose, again as known from phased-array theory [22]. In our tests, scans to ±60° roughly doubled the beamwidth, consistent with the expected cosθ effect [22]. These behaviours indicate the model correctly captures key phased-array physics.

Using SNR feedback to select beams proved effective. The algorithm prioritized satellites with the strongest signals, maintaining high link quality for those beams. This method is common in communication systems: higher SNR means a better link. By dynamically swapping beams when another satellite's SNR became superior, the system continually optimized performance. This demonstrates the utility of SNR-based beam assignment. In real-world terms, it means the ground terminal would focus on the clearest targets, enhancing throughput. Our results suggest that multi-beam tracking with SNR selection can robustly maintain optimal links under ideal conditions.

Some practical observations emerged from the simulation. When multiple beams were active, the total available power divided among them, slightly reducing the gain per beam. The patterns indicated small interference where beams overlapped, suggesting that more advanced beam-shaping or null-steering techniques could help. The simulation used uniform weighting, so sidelobe levels were moderate. Future work could experiment with tapering to lower sidelobes and improve isolation between beams. The array was modelled with half-wavelength spacing, which prevented grating lobes. If spacing were larger, grating lobes would appear at high scan angles. Including such effects in future simulations would be instructive.

Quantitative metrics were not fully evaluated and should be addressed in future work. For example, explicitly measuring each beam's HPBW and sidelobe levels would clarify performance. The current results are largely qualitative, based on pattern plots. A more thorough analysis could compute dB values of sidelobes or beam efficiencies. Additionally, performance under realistic conditions needs exploration. The model assumed ideal propagation with no noise aside from the nominal SNR calculation and no Doppler shift. Atmospheric losses and Doppler effect would affect link SNR. Incorporating these factors would show how robust the tracking is in practice. Also, the simulation used discrete time updates; testing finer time resolution could improve stability. In summary, the simulation behaved as expected and confirmed the phased-array tracking concept but extending it with detailed metrics and real-world impairments would strengthen the analysis.

7 Conclusions, Recommendations and Future Work

7.1 Conclusions and Recommendations

This project developed and tested a simulation framework for multi-beam phased array antennas, with a focus on LEO satellite tracking. The simulation framework demonstrated effective single-beam and multi-beam steering under controlled, ideal conditions. Performance trends matched theoretical predictions. For example, increasing the operating frequency and array size resulted in narrower beamwidths and improved spatial resolution, consistent with array theory.

Key behaviours were observed during the tests:

Beam steering up to ±60° from boresight was achieved with acceptable gain loss.

Side lobe levels remained below -13 dB during single beam steering simulations at 30 GHz.

Grating lobes began to appear when element spacing exceeded half-wavelength, especially at large scan angles.

Multi-beam operation introduced minor gain reductions and higher side lobe floors, suggesting a need for future adaptive weighting techniques.

The simulations assumed ideal free-space conditions without atmospheric losses, Doppler effects, or environmental noise. This assumption allowed early validation of

phased array concepts but limits the direct application of the current results to real-world satellite operations. Nevertheless, critical behaviours such as grating lobe formation, side lobe growth, and beam distortion at high steering angles were accurately captured, reinforcing the validity of the core model.

The project successfully created a strong foundation for future real-world ground station designs. Although the current system cannot yet handle dynamic, real-time satellite tracking, it provides a modular base ready for extension. Future improvements—including environmental modelling, hardware constraints, and optimization techniques—could transform the simulation into a complete, deployable satellite tracking system. With further development, the framework could help reduce the time, cost, and complexity of next-generation LEO and VLEO ground terminals.

7.2 Future Work

The simulation framework built for phased array satellite tracking shows strong potential. However, the tests so far were carried out under ideal conditions without real-world challenges. The model has not yet been validated using live satellite tracking or dynamic link conditions.

Several areas for future work have been identified to extend and improve the project. Expanding the simulation in these ways would not only increase confidence in system performance but also highlight key limitations and areas for optimisation.

- One important step would be to add real-world environmental effects into the model. The current simulation assumes free-space propagation without considering weather, atmospheric losses, or Doppler shifts. These effects become critical at high frequencies, especially above 30 GHz, and can impact beam stability and link quality. Including them would make the simulation a much closer match to real operating environments.
- Another area for improvement is investigating specific case studies involving real satellite missions. Very Low Earth Orbit (VLEO) satellites move faster than traditional LEO satellites and experience stronger atmospheric drag. Their faster handover times create challenges for tracking and beam management. Testing the simulation against VLEO mission profiles would show how well the system handles rapid changes and could guide future ground station designs.

- Improving the accuracy of the simulation itself would also be valuable. Adding more advanced modelling techniques, such as full electromagnetic propagation models or RF channel simulations, would better capture real-world effects across different environments. These improvements would provide higher confidence in the results.

In addition to the simulation model, hardware aspects could be considered. Incorporating limitations from phased array electronics, such as amplifier non-linearities, element failures, or real-time beamforming hardware constraints, would help bridge the gap between simulation and real-world deployment.
Finally, linking the simulation framework to a full mission design study could add significant value. Factors like ground station layout, tracking handover strategies, power budgets, and data link margins could be modelled to create a complete ground terminal concept. Exploring dynamic scheduling, beam management for large satellite constellations, and system-level optimisation would push the project toward operational readiness.
Expanding the simulation framework with these upgrades could move the project from basic system testing to a fully functional real-time tracking platform. With further development, the system could eventually support operational LEO and VLEO satellite networks, helping reduce the time, cost, and complexity of future satellite ground terminals.

References

[1] D. I. Group, “Satellite communications: what’s the difference between LEO, MEO and GSO?,” 2021. [Online]. Available: https://www.darwininnovationsgroup.com/. [Accessed 12 04 2025].

[2] Space.com, “Starlink satellites: Facts, tracking and impact on astronomy,” 28 03 2025. [Online]. Available: https://www.space.com/starlink-satellites. [Accessed 12 04 2025].

[3] N. S. S. S. V. Institute, “State-of-the-Art of Small Spacecraft Technology,” NASA, 2022. [Online]. Available: https://www.nasa.gov/smallsat-institute. [Accessed 12 04 2025].

[4] C. A. Balanis, ANTENNA THEORY THIRD EDITION, New Jersey: A JOHN WILEY & SONS, 2005.

[5] R. J. Mailloux, Phased Array Antenna Handbook Second Edition, Norwood, Massachusetts: ARTECH HOUSE, INC, 2008.

[6] H. W. M. Z. a. S. Y. G. He, “A Review of Multibeam Phased Array Antennas as LEO Satellite Constellation Ground Station,” *IEEE Access,* vol. vol 9., p. pp. 144830–144846, 2021.

[7] J. M. S. a. B. D. M. C. I. Adomnitei, “The Design and Implementation of a Phased Antenna Array System for LEO Satellite Communications,” *Sensors,* vol. vol. 24, no. no. 6, p. p. 1915, 2024.

[8] K. L. a. Y. A. E. C. K. Ng, “Modelling and Simulation of Phased Array Antenna for LEO Satellite Tracking,” in *Proc. International Conference on Information Networking (ICOIN)*, 2002.

[9] M. I. Skolnik, Introduction to Radar Systems, New York, NY, USA: McGraw-Hill, 2021.

[10] M. A. Richards, Fundamentals of Radar Signal Processing, New York, NY, USA: McGraw-Hill, 2014.

[11] B. B. a. J. K. Peter Delos, “Phased Array Antenna Patterns—Part 1: Linear Array Beam Characteristics and Array Factor,” Analog Devices, 2020. [Online]. Available: https://www.analog.com/en/resources/analog-dialogue/articles/phased-array-antenna-patterns-part1.html#:~:text=,the%20number%20of%20elements%20increases. [Accessed 12 04 2025].

[12] N. J. T. Report, “Phased Array Beamforming,” NASA, 1974.

[13] R. R. e. al, “Digital Beamforming Radar (DBSAR): Performance Analysis During Eco-3D Campaign,” NASA Technical Memo, 2014.

[14] D. Systèmes, “Electromagnetic Field Simulation Software, official documentation,” CST Studio Suite, [Online]. Available: https://www.3ds.com/products/simulia/cst-studio-suite. [Accessed 12 04 2025].

[15] MathWorks, “Phased Array System Toolbox,” MATLAB official documentation, [Online]. Available: https://uk.mathworks.com/help/phased/index.html. [Accessed 12 04 2025].

[16] A. Inc, “3D High Frequency Simulation Software, official documentation,” Ansys HFSS, [Online]. Available: https://www.ansys.com/products/electronics/ansys-hfss#:~:text=Ansys%20HFSS%20is%20a%203D,worldwide%20use%20Ansys%20HFSS%20software. [Accessed 12 04 2025].

[17] I. G. I. o. E. o. A. a. I. Systems, “Ethically Aligned Design: A Vision for Prioritizing Human Well-being with Autonomous and Intelligent Systems,” IEEE Standards Association, 2019.

[18] M. J. Peterson, “space Faring and Space Security: Ethical Challenges,” *Science and Engineering Ethics,* vol. vol. 23, no. no. 2, p. pp. 473–491, 2017.

[19] C. L. C. a. J. J. Wenzel, “The Dual-Use Dilemma for Satellite Communications and Earth Observation Systems,” *IEEE Aerospace and Electronic Systems Magazine,* vol. vol. 35, no. no. 4, p. pp. 18–24, 2020.

[20] I. T. U. (ITU, “Radio Regulations: Articles and Appendices,” ITU, 2020.

[21] CelesTrak, “CelesTrak: Satellite Tracking and Data Resources,” [Online]. Available: https://www.celestrak.com/. [Accessed 12 04 2025].

[22] P. D. a. B. B. a. J. Kraft, “Phased-Array Antenna Patterns (Part 3)—Linear-Array Beam Characteristics and Array Factor,” Microwaves & RF, 17 8 2020. [Online]. Available: https://www.mwrf.com/technologies/embedded/systems/article/21139283/analog-devices-phased-array-antenna-patterns-part-3linear-array-beam-characteristics-and-array-factor. [Accessed 12 04 2025].

Appendices

Appendix A – Project brief and project files

GitHub project QR code

SCAN ME

Gantt Chart

GCU Glasgow Caledonian University

University for the Common Good

SCHOOL OF COMPUTING, ENGINEERING & BUILT ENVIRONMENT
BACHELOR OF ENGINEERING

EEE Honours Research Project Proposal Form

PROJECT ACTIVITIES GANTT CHART

ACTIVITY	Duration (1 Div. = 1 Week)																												
	TnAWk1	TnAWk2	TnAWk3	TnAWk4	TnAWk5	TnAWk6	TnAWk7	TnAWk8	TnAWk9	TnAWk10	TnAWk11	TnAWk12	TnASmdyWk1	TnASmdyWk2	TnASmdyWk3	TnBWk1	TnBWk2	TnBWk3	TnBWk4	TnBWk5	TnBWk6	TnBWk7	TnBWk8	TnBWk9	TnBWk10	TnBWk11	TnBWk12	TnBSmdyWk1	Thesis Submission & Oral/poster Week
Initial research and Project Proposal																													
Literature Review on Sat Comm & Phased Array Antennas																													
Design and Simulation of a Single Antenna Element																													
Development of a Phased Array Antenna																													
Beamforming and Beam Steering Simulation																													
Performance Analysis of the Phased Array Antenna																													
Comparison with Traditional Antenna Systems																													
Documentation of findings and Logbook																													
Final Report Writing																													
Poster																													

Project Brief

BRIEF INTRODUCTION, PROPOSED PROBLEM STATEMENT AND PLAN

The main part of this project will be a simulation of each aim to create results for phased array antennas and beam forming. This research and simulation will allow improvement on current designs.

Traditional satellite communication systems have limitations of mechanically steered antennas, which limits real-time tracking and bandwidth optimization. An example of this limitation is ground station to LEO satellites where the speed, high throughput, and multi-satellite tracking become impossible.

Examples of systems that cannot function without phased array antennas and beamforming are StarLink and OneWeb.

Simulations will be done in MatLab and/or CST Studio Suite; this will have to be decided based on availability of licenses. (This will also change based on whether the focus will be signal processing or 3D electromagnetic analysis.)

The plan will follow the aims in order and attempt to keep time with the Gantt chart, and each step will be logged with research and findings.

Once the main aims are complete, work on different configurations like frequencies, element spacing, and steering angles can be done to attempt to further current research.

Finally explaining the improvements and how they improve current methods.

Appendix B - MATLAB Code for Graphs and Figures

Polar_Cart_plot MATLAB code

```
% Angle (0 to 360 degrees)
theta = linspace(0, 2*pi, 1000);  % radians

% Radiation Pattern of Half-wave Dipole: E(theta) = sin(theta)
E = abs(sin(theta));

% Convert to dB Scale
```

```
E_dB = 20*log10(E / max(E));
E_dB(E_dB < -40) = -40;  % Limit floor for display clarity

%% Cartesian Plot
figure;
plot(rad2deg(theta), E_dB, 'b', 'LineWidth', 1.5);
grid on;
xlabel('Angle (degrees)');
ylabel('Gain (dB)');
title('Half-wave Dipole Radiation Pattern (Cartesian Plot)');
xlim([0 360]);
ylim([-40 0]);

%% Polar Plot
figure;
polarplot(theta, E_dB, 'b', 'LineWidth', 1.5);
ax = gca;
ax.ThetaZeroLocation = 'top';
ax.ThetaDir = 'clockwise';
rlim([-40 0]);
title('Half-wave Dipole Radiation Pattern (Polar Plot)');
```

Three-dimensional radiation pattern of a half-wave dipole antenna MATLAB code

```
% Resolution of theta and phi
theta = linspace(0, pi, 40);
phi = linspace(0, 2*pi, 40);
[theta, phi] = meshgrid(theta, phi);

% Dipole radiation pattern (normalized)
r = abs(sin(theta));

% Cut-out section from 270 to 360 degrees
cut_phi_min = 3*pi/2;    % 270 degrees
cut_phi_max = 2*pi;      % 360 degrees
cut_index = (phi >= cut_phi_min) & (phi <= cut_phi_max);
r(cut_index) = NaN;

% Convert spherical to Cartesian coordinates
x = r .* sin(theta) .* cos(phi);
y = r .* sin(theta) .* sin(phi);
z = r .* cos(theta);

% Plot 3D Radiation Pattern
figure('Color', 'w')
surf(x, y, z, r, 'EdgeColor', [0.5 0.5 0.5], 'LineWidth', 0.5);
colormap('parula')
alpha(0.9)

% Lighting for better 3D appearance
light
lighting gouraud
material shiny

hold on
```

```
%Dipole in the middle (along z-axis)
L = 1; % Length of dipole
plot3([0 0], [0 0], [-L/2 L/2], 'k', 'LineWidth', 3); % Black line dipole

% Add Label to Dipole
text(0, 0, L/2 + 0.1, 'Dipole', 'HorizontalAlignment', 'center', ...
    'FontSize', 12, 'FontWeight', 'bold', 'Color', 'k')

hold off

axis equal
xlabel('X-axis')
ylabel('Y-axis')
zlabel('Z-axis')

grid on
view(45, 30)
```

Beam Width Plot

```
% Angle range (-90 to 90 degrees)
theta = linspace(-90, 90, 1000);

% Create main lobe with side lobes using sinc function centered at 30°
main_lobe = abs(sinc((theta - 30) / 20));

% Convert to dB scale
main_lobe_dB = 20 * log10(main_lobe / max(main_lobe));
main_lobe_dB(main_lobe_dB < -40) = -40;  % Limit floor for clarity

% Define HPBW and FNBW markers
HPBW_left = 20;    % Left -3 dB point
HPBW_right = 40;   % Right -3 dB point
FNBW_left = 10;    % First null left
FNBW_right = 50;   % First null right

% Plot the radiation pattern
figure;
plot(theta, main_lobe_dB, 'b', 'LineWidth', 2);
hold on;

% Add -3 dB line
yline(-3, '--', 'Color', [0.5 0.2 0], 'LineWidth', 1.5);
text(2, -1, '3 dB', 'Color', [0.5 0.2 0], 'FontSize', 10,
'HorizontalAlignment', 'center');
annotation('arrow', [0.5 0.5], [0.55 0.61], 'Color', [0.5 0.2 0],
'LineWidth', 1.5);


% Add HPBW markers
xline(HPBW_left, '--g', 'LineWidth', 1);
xline(HPBW_right, '--g', 'LineWidth', 1);
annotation('doublearrow', [0.605 0.69], [0.47 0.47], 'Color', 'g');
text(30, -7, 'HPBW', 'Color', 'g', 'FontSize', 10, 'HorizontalAlignment',
'center');

% Add FNBW markers
```

```
xline(FNBW_left, '--m', 'LineWidth', 1);
xline(FNBW_right, '--m', 'LineWidth', 1);
annotation('doublearrow', [0.56 0.73], [0.33 0.33], 'Color', 'm');
text(30, -28, 'FNBW', 'Color', 'm', 'FontSize', 10, 'HorizontalAlignment',
'center');

grid on;
xlabel('Angle (Degrees)');
ylabel('Amplitude (dB)');
title('Definition of Antenna Beamwidth (Main Lobe at 30°)');
xlim([-90 90]);
ylim([-40 20]);
```

Appendix C – MATLAB Code for Single Beam Simulation

```
close all  % Close all figures
clc        % Clear the Command Window

%% -------------------- Constants --------------------
f = 30e9;                 % Frequency of operation (30 GHz for Ka-band LEO
satellite comms)
lambda = 3e8 / f;         % Wavelength (meters)
k = 2 * pi / lambda;      % Wavenumber (radians per meter)

%% -------------------- Array Configuration --------------------
M = 20;                   % Number of elements along the X-axis
N = 20;                   % Number of elements along the Z-axis
dx = lambda / 2;          % Element spacing in X-direction (λ/2)
dz = lambda / 2;          % Element spacing in Z-direction (λ/2)

%% -------------------- Beam Steering Angles --------------------
phiMax = 0;              % Desired azimuth steering angle (degrees)
thetaMax = 90;           % Desired elevation steering angle (degrees)

% Compute phase shifts needed for beam steering
alphaX = -k * dx * cosd(phiMax); % Phase gradient in X
alphaZ = -k * dz * cosd(thetaMax); % Phase gradient in Z

%% -------------------- Array Factor Calculation --------------------
% Define angular ranges
phi = linspace(0, pi, 500);    % Azimuth angle vector
```

```
theta = linspace(0, pi, 500);  % Elevation angle vector

% Compute array factor along X-axis
phiX = k * dx * cos(phi) + alphaX;
AFx = 1;
for i = 1:M-1
    AFx = AFx + exp(1i * i * phiX);
end
if M == 1
    AFx = ones(1, length(phi));
end

% Compute array factor along Z-axis
phiZ = k * dz * cos(theta) + alphaZ;
AFz = 1;
for i = 1:N-1
    AFz = AFz + exp(1i * i * phiZ);
end
if N == 1
    AFz = ones(1, length(theta));
end

% Compute total array factor (outer product of AFx and AFz)
AF = zeros(length(phi), length(theta));
for g = 1:length(theta)
    for f = 1:length(phi)
        AF(f, g) = AFx(f) * AFz(g);
    end
end

%% -------------------- Radiation Pattern Plot --------------------
[thetaGrid, phiGrid] = meshgrid(theta, phi);  % Create 2D angle grid

% Convert spherical to Cartesian coordinates for plotting
x = abs(AF) .* sin(thetaGrid) .* cos(phiGrid);
y = abs(AF) .* sin(thetaGrid) .* sin(phiGrid);
z = abs(AF) .* cos(thetaGrid);

% Plot 3D radiation pattern
figure('units','normalized','outerposition',[0 0 1 1])
```

```
mesh(x, y, z, abs(AF))
axis equal
xlabel('x')
ylabel('y')
zlabel('z')
xlim([-500 500])
ylim([-500 500])
zlim([-500 500])
title(['LEO Satellite Beamforming | Elevation = ' num2str(thetaMax) '°,
Azimuth = ' num2str(phiMax) '°']);
view(145, 20)
```

Appendix D – MATLAB Code for Multi-Beam Simulation

```
close all  % Close all open figure windows
clc        % Clear the Command Window

%% -------------------- Constants --------------------
f = 30e9;                 % Frequency of operation (30 GHz for Ka-band LEO
satellite comms)
lambda = 3e8 / f;         % Wavelength (meters)
k = 2 * pi / lambda;      % Wavenumber (radians per meter)

%% -------------------- Array Configuration --------------------
M = 20;                   % Number of elements along the X-axis
N = 20;                   % Number of elements along the Z-axis
dx = lambda / 2;          % Element spacing in X-direction (λ/2)
dz = lambda / 2;          % Element spacing in Z-direction (λ/2)

%% -------------------- User Input for Multiple Satellite Directions ------
--------------
numBeams = input('Enter number of satellites (beams): ');
phiMaxArray = zeros(1, numBeams);       % Azimuth angles (°)
thetaMaxArray = zeros(1, numBeams);     % Elevation angles (°)
weights = ones(1, numBeams);            % Uniform weights for all beams

for b = 1:numBeams
    phiMaxArray(b) = input(['Enter azimuth angle (°) for beam ' num2str(b)
': ']);
```

```
    thetaMaxArray(b) = input(['Enter elevation angle (°) for beam '
num2str(b) ': ']);
end

%% -------------------- Define Scanning Grid --------------------
phi = linspace(0, pi, 500);         % Azimuth scan (radians)
theta = linspace(0, pi, 500);       % Elevation scan (radians)

%% -------------------- Total Array Factor Initialization ----------------
---
AF_total = zeros(length(phi), length(theta));

%% -------------------- Loop Over Beams --------------------
for b = 1:numBeams
    % Compute beam steering phase shifts
    alphaX = -k * dx * cosd(phiMaxArray(b));
    alphaZ = -k * dz * cosd(thetaMaxArray(b));

    % Calculate array factor for X-axis
    phiX = k * dx * cos(phi) + alphaX;
    AFx = 1;
    for m = 1:M-1
        AFx = AFx + exp(1i * m * phiX);
    end
    if M == 1
        AFx = ones(1, length(phi));
    end

    % Calculate array factor for Z-axis
    phiZ = k * dz * cos(theta) + alphaZ;
    AFz = 1;
    for n = 1:N-1
        AFz = AFz + exp(1i * n * phiZ);
    end
    if N == 1
        AFz = ones(1, length(theta));
    end

    % Combine to form 2D array factor for this beam
    AF_beam = (AFx.' * AFz) * weights(b);
```

```
    % Add to total array factor (superposition)
    AF_total = AF_total + abs(AF_beam);
end

%% -------------------- Convert to Cartesian and Plot --------------------
[theta_grid, phi_grid] = meshgrid(theta, phi);
x = abs(AF_total) .* sin(theta_grid) .* cos(phi_grid);
y = abs(AF_total) .* sin(theta_grid) .* sin(phi_grid);
z = abs(AF_total) .* cos(theta_grid);

figure('units', 'normalized', 'outerposition', [0 0 1 1]);
mesh(x, y, z, abs(AF_total)); % 3D plot
axis equal;
xlabel('x');
ylabel('y');
zlabel('z');
title(['Multi-Beam Antenna Pattern for ', num2str(numBeams), '
Satellites']);
xlim([-500 500]);
ylim([-500 500]);
zlim([-500 500]);
colorbar;
view(145, 20);
```

Appendix E – MATLAB Code for Reading TLE Files

```
function [sat_labels, line1_data, line2_data] = readTLEfile(tleFile,
numBeams)
    % readTLEfile: Extracts satellite identifiers and TLE lines from a text
file.
    %
    % INPUTS:
    %   tleFile   - Path to the TLE text file (e.g.,
'celestrak_TLE_DATA.txt')
    %   numBeams  - Number of satellites (i.e., number of 3-line TLE blocks
to read)
    %
    % OUTPUTS:
```

```
    %   sat_labels - Cell array containing satellite names
    %   line1_data - Cell array of TLE Line 1 strings
    %   line2_data - Cell array of TLE Line 2 strings

    fid = fopen(tleFile, 'r');                      % Open file
    tle_lines = textscan(fid, '%s', 'Delimiter', '\n');
    fclose(fid);                                    % Close file after
reading
    tle_lines = tle_lines{1};                       % Extract cell array of
lines

    % Preallocate output arrays
    sat_labels = cell(1, numBeams);
    line1_data = cell(1, numBeams);
    line2_data = cell(1, numBeams);

    for i = 1:numBeams
        baseIdx = (i - 1) * 3;
        sat_labels{i} = strtrim(tle_lines{baseIdx + 1});  % Satellite name
        line1_data{i} = tle_lines{baseIdx + 2};           % Line 1
        line2_data{i} = tle_lines{baseIdx + 3};           % Line 2
    end
end
```

Appendix F – TLE files used [21]

Russian LEO Navigation

```
COSMOS 2361
1 25590U 98076A   25085.24608917  .00000132  00000+0  12624-3 0  9991
2 25590  82.9383 177.4391 0030059 272.7097 145.0986 13.73184118315525
COSMOS 2378
1 26818U 01023A   25085.18660022  .00000135  00000+0  12706-3 0  9993
2 26818  82.9311 193.6081 0032366 213.2304 192.8336 13.74111463193381
COSMOS 2389
1 27436U 02026A   25085.19348900  .00000131  00000+0  11932-3 0  9999
2 27436  82.9508 140.5863 0047737  70.6430 343.7993 13.75125758145609
COSMOS 2398
1 27818U 03023A   25084.84546126  .00000131  00000+0  12613-3 0  9999
2 27818  82.9440 105.7127 0032650 119.0422  53.2115 13.72355874 92242
```

```
COSMOS 2407
1 28380U 04028A   25084.95750272  .00000162  00000+0  14895-3 0  9999
2 28380  82.9607  46.7582 0040592  66.7820  39.8503 13.76280172 38226
COSMOS 2414
1 28521U 05002A   25085.19269868  .00000189  00000+0  14453-3 0  9991
2 28521  82.9533  22.4670 0040386 164.8838 195.3543 13.87862516 22001
COSMOS 2429
1 32052U 07038A   25085.21640086  .00000128  00000+0  11662-3 0  9996
2 32052  82.9847 176.0528 0039320  48.1695 312.2807 13.75117343880173
COSMOS 2454
1 35635U 09039A   25085.23435794  .00000186  00000+0  13790-3 0  9997
2 35635  82.9610   6.9045 0020649  99.9426  53.8459 13.89887942795367
COSMOS 2463
1 36519U 10017A   25084.63367494  .00000131  00000+0  12883-3 0  9993
2 36519  82.9616 219.2629 0034899 295.5188  74.7762 13.71619060746532
```

CubeSats(Limited to 100)

```
CUTE-1 (CO-55)
1 27844U 03031E   25076.57033365  .00001015  00000+0  46214-3 0  9990
2 27844  98.6795  85.9207 0010833  73.8545 286.3825 14.23876256126680
CUBESAT XI-IV (CO-57)
1 27848U 03031J   25076.47987407  .00000857  00000+0  39808-3 0  9992
2 27848  98.6822  85.8997 0010779  89.0034 271.2380 14.23228145126408
CUBESAT XI-V
1 28895U 05043F   25076.36420948  .00005592  00000+0  92984-3 0  9995
2 28895  98.2353 219.7530 0014534 210.2938 149.7428 14.70436052 34568
CUTE-1.7+APD II (CO-65)
1 32785U 08021C   25076.43466474  .00013246  00000+0  98858-3 0  9990
2 32785  97.7790  47.0969 0012526 126.3107 233.9276 15.02910019916430
AAUSAT-II
1 32788U 08021F   25076.49348330  .00195179  00000+0  27074-2 0  9996
2 32788  97.6063  69.9715 0004057 112.2578 247.9107 15.56364496920178
CANX-2
1 32790U 08021H   25076.45342322  .00011236  00000+0  89515-3 0  9990
2 32790  97.8054  45.6599 0014443 117.2023 243.0674 15.00443640916195
SEEDS II (CO-66)
1 32791U 08021J   25076.42582506  .00028183  00000+0  14921-2 0  9995
2 32791  97.7226  54.7980 0007091  95.6089 264.5952 15.15365960917735
SWISSCUBE
```

```
1 35932U 09051B   25076.60855474  .00003355  00000+0  69421-3 0  9996
2 35932  98.4394 331.2497 0006618 181.6783 178.4396 14.60961216822450
BEESAT-1
1 35933U 09051C   25076.61900199  .00002834  00000+0  59486-3 0  9994
2 35933  98.4325 331.7610 0004809 192.4745 167.6336 14.60431519822514
ITUPSAT1
1 35935U 09051E   25076.63588802  .00002581  00000+0  55677-3 0  9998
2 35935  98.4421 331.3865 0006849 205.5058 154.5804 14.59254906822123
TISAT 1
1 36799U 10035E   25076.53246301  .00026316  00000+0  14716-2 0  9995
2 36799  98.0637 345.5161 0005246  50.4738 309.6955 15.13444410798242
AEROCUBE 4.5A
1 38767U 12048K   25076.59077419  .00045042  00000+0  14066-2 0  9991
2 38767  64.6490 144.3447 0106435 297.7727  61.2642 15.27494920301962
STRAND-1
1 39090U 13009E   25076.47984751  .00001104  00000+0  38906-3 0  9993
2 39090  98.3818 263.3834 0009334 150.2859 209.8860 14.36697270631477
BRITE-AUSTRIA
1 39091U 13009F   25076.45651688  .00000728  00000+0  26393-3 0  9990
2 39091  98.3872 262.6253 0010686 158.2928 201.8713 14.36228503631481
NEE-01 PEGASO
1 39151U 13018B   25076.33142333  .00008449  00000+0  88260-3 0  9995
2 39151  98.0587 203.4083 0013314 223.5870 136.4296 14.89887863642585
ESTCUBE 1
1 39161U 13021C   25076.61765706  .00004840  00000+0  65867-3 0  9995
2 39161  97.7897 140.7576 0009701  68.5609 291.6637 14.79165073637474
POPACS 1
1 39268U 13055D   25076.60366400  .00069284  44406-6  77488-3 0  9997
2 39268  80.9781 189.4919 0285019 270.5887  86.2699 15.26263283601764
POPACS 2
1 39269U 13055E   25076.62085650  .00027803  00000+0  56764-3 0  9995
2 39269  80.9952 299.2863 0492709 199.8984 158.2407 14.71610850595607
POPACS 3
1 39270U 13055F   25076.53699362  .00027555  00000+0  70859-3 0  9993
2 39270  81.0098   0.4754 0594314  10.7871 350.5424 14.45454344572330
ZACUBE-1 (TSHEPISOSAT)
1 39417U 13066B   25076.45005814  .00013814  00000+0  12338-2 0  9992
2 39417  97.7721  34.0262 0044649 335.8507  24.0620 14.95268288612336
WNISAT-1
1 39423U 13066H   25076.53353146  .00003636  00000+0  68400-3 0  9995
```

2 39423 97.6720 254.9774 0165433 229.6878 128.9768 14.56725263600217
TRITON-1
1 39427U 13066M   25076.49670397 .00008260 00000+0 10631-2 0 9994
2 39427 97.8395 352.4341 0094095 279.5752 79.4837 14.78253497606532
DELFI-N3XT
1 39428U 13066N   25076.34769032 .00017769 00000+0 18805-2 0 9999
2 39428 97.8366 355.0404 0085748 278.1629 80.9867 14.86510524606551
GOMX-1
1 39430U 13066Q   25076.61536645 .00004858 00000+0 76187-3 0 9997
2 39430 97.6952 300.4023 0135090 100.9797 260.6639 14.67080527602912
CUBEBUG-2 (LO-74)
1 39440U 13066AA 25076.56917218 .00010874 00000+0 11250-2 0 9995
2 39440 97.8426 21.8135 0065528 96.8102 264.0577 14.88650223608936
NEE-02 KRYSAOR
1 39441U 13066AB 25076.57586516 .00006546 00000+0 76544-3 0 9999
2 39441 97.8495 16.2537 0071386 123.9435 236.8592 14.83581837608424
FUNCUBE-1 (AO-73)
1 39444U 13066AE 25076.44644838 .00019898 00000+0 15638-2 0 9990
2 39444 97.7614 38.2385 0039874 313.0010 46.7873 15.00274411610960
UWE-3
1 39446U 13066AG 25076.59504911 .00013380 00000+0 12979-2 0 9990
2 39446 97.8157 28.0922 0056022 39.3159 321.2107 14.91592537609381
BRITE-CA1 (TORONTO)
1 40020U 14033L   25076.31988010 .00003084 00000+0 48425-3 0 9997
2 40020 97.9104 210.8071 0079521 299.5650 59.7647 14.71222726575006
DUCHIFAT-1
1 40021U 14033M   25076.48081856 .00042464 00000+0 17835-2 0 9993
2 40021 98.1011 83.7910 0007175 237.4091 122.6452 15.23295162585492
NANOSATC-BR1
1 40024U 14033Q   25076.50616081 .00027850 00000+0 14889-2 0 9991
2 40024 98.0906 68.7818 0004009 358.8621   1.2599 15.15041749584468
QB50P1
1 40025U 14033R   25076.49598156 .00020626 00000+0 13296-2 0 9997
2 40025 98.0773 54.5616 0010455 352.8629   7.2447 15.08304093583951
QB50P2
1 40032U 14033Y   25076.48186770 .00017145 00000+0 11663-2 0 9997
2 40032 98.0365 44.1525 0006482 292.2927 67.7611 15.06381519583706
PERSEUS-M2
1 40037U 14033AD 25076.62252332 .00005457 00000+0 52764-3 0 9997
2 40037 97.9491 15.2165 0012960 19.6027 340.5687 14.93152165582597

PERSEUS-M1
1 40039U 14033AF 25076.60699046 .00005783 00000+0 55964-3 0 9991
2 40039 97.9242 10.4315 0012733 18.6773 341.4910 14.93096272582441
POLYITAN-1
1 40042U 14033AJ 25076.47340978 .00030529 00000+0 16319-2 0 9993
2 40042 98.1012 60.9864 0007668 296.4751 63.5692 15.15007418584030
TIGRISAT
1 40043U 14033AK 25076.44702732 .00008199 00000+0 10078-2 0 9995
2 40043 97.7234 234.5173 0053076 131.0528 229.5290 14.82261007577897
AEROCUBE 6A
1 40045U 14033AM 25076.41153447 .00016236 00000+0 16273-2 0 9991
2 40045 97.6853 246.7681 0045054 100.4055 260.2245 14.90661928578399
AEROCUBE 6B
1 40046U 14033AN 25076.40350548 .00016667 00000+0 16272-2 0 9999
2 40046 97.6825 245.7661 0043518 94.4593 266.1600 14.91752390578472
CANX-4
1 40055U 14034C   25076.58539853 .00003023 00000+0 40774-3 0 9994
2 40055 98.3731 288.8107 0013863 40.7613 319.4632 14.79872590576966
CANX-5
1 40056U 14034D   25076.58855620 .00003045 00000+0 41051-3 0 9991
2 40056 98.3734 288.8316 0013855 40.9147 319.3101 14.79885404567774
UKUBE-1
1 40074U 14037F   25076.43439241 .00021049 00000+0 15636-2 0 9998
2 40074 98.3842 31.5678 0000532 87.8248 272.3035 15.03050023579695
BRITE-PL2 (HEWELIUSZ)
1 40119U 14049B   25076.53812810 .00005810 00000+0 57899-3 0 9995
2 40119 97.8825 181.6667 0015054 178.8689 181.2566 14.91893512573291
AEROCUBE 5C
1 40965U 15058B   25076.60743567 .00012366 00000+0 10329-2 0 9995
2 40965 64.7679 239.2398 0176465 226.4487 132.1856 14.87465014297647
AEROCUBE 7
1 40966U 15058C   25076.58301119 .00015404 00000+0 12098-2 0 9997
2 40966 64.7647 229.8390 0168939 226.2992 132.4023 14.90454414297775
FOX-1A (AO-85)
1 40967U 15058D   25076.56940669 .00011033 00000+0 94642-3 0 9995
2 40967 64.7750 254.2108 0173351 221.8402 136.9352 14.86933139 45575
SINOD-D 1
1 40968U 15058E   25076.59077822 .00016394 00000+0 13093-2 0 9996
2 40968 64.7756 243.4379 0164148 220.8690 138.0021 14.90368474 48471
SNAP-3 ALICE

1 40970U 15058G   25076.62482434 .00048619 00000+0 22265-2 0 9998
2 40970 64.7656 177.3002 0108936 220.8055 138.4876 15.14993403 46922
LMRST-SAT
1 40971U 15058H   25076.62980923 .00011108 00000+0 95135-3 0 9995
2 40971 64.7752 249.6658 0175361 223.2344 135.4892 14.86750515 45583
SNAP-3 EDDIE
1 40972U 15058J   25076.62885293 .00052347 00000+0 23662-2 0 9995
2 40972 64.7629 170.0769 0108232 221.9861 137.2931 15.15465880 49038
PROPCUBE 3
1 40973U 15058K   25076.58635178 .00015097 00000+0 12131-2 0 9996
2 40973 64.7692 234.5371 0170428 224.9143 133.8076 14.89467297 46679
BISONSAT
1 40974U 15058L   25076.60046973 .00034871 00000+0 21032-2 0 9990
2 40974 64.7651 195.4563 0137015 223.3403 135.6877 15.02985573 46688
SNAP-3 JIMI
1 40975U 15058M   25076.50843865 .00022218 00000+0 15944-2 0 9992
2 40975 64.7674 217.2766 0156592 224.1892 134.6629 14.94926782 45774
PROPCUBE 1 (FLORA)
1 40976U 15058N   25076.58240020 .00008815 00000+0 78758-3 0 9995
2 40976 64.7740 266.8502 0174722 224.7511 133.9394 14.85441346 48341
SINOD-D 3
1 40977U 15058P   25076.62466760 .00013687 00000+0 11382-2 0 9994
2 40977 64.7724 256.5378 0165649 224.0717 134.7095 14.88823325 46653
HORYU-4
1 41340U 16012D   25076.05542069 .00037366 00000+0 11821-2 0 9992
2 41340 30.9986 338.4047 0008347 272.1444 87.8245 15.31535203499794
RAVAN
1 41849U 16067B   25076.54070954 .00027365 00000+0 10374-2 0 9999
2 41849 98.0530 278.7621 0010243 166.2669 193.8848 15.26808522457503
CELTEE 1
1 41850U 16067C   25076.49737323 .00012963 00000+0 73602-3 0 9997
2 41850 98.1091 267.6650 0001099 40.9294 319.2018 15.13077851456666
OPTICUBE 04
1 41851U 16067D   25076.49056000 .00007053 00000+0 48149-3 0 9996
2 41851 98.0924 260.0114 0016139 215.1597 144.8565 15.06431231456337
AEROCUBE 8D
1 41852U 16067E   25076.48269250 .00016947 00000+0 89301-3 0 9996
2 41852 98.1134 268.3881 0003680 261.4344 98.6470 15.15670804456685
AEROCUBE 8C
1 41853U 16067F   25076.49469580 .00016904 00000+0 88830-3 0 9995

2 41853 98.0971 266.3541 0006583 187.4241 172.6893 15.15755425456677
PROMETHEUS 2-1
1 41854U 16067G   25076.49668653 .00062036 00000+0 15954-2 0 9991
2 41854 98.0885 280.5194 0008054 190.5051 169.6025 15.39015237457437
PROMETHEUS 2-3
1 41855U 16067H   25076.50466085 .00061158 00000+0 15766-2 0 9994
2 41855 98.0827 279.7592 0007002 200.0854 160.0115 15.38953425457430
CORVUS BC2
1 42846U 17042X   25076.46606797 .00008684 00000+0 66699-3 0 9997
2 42846 97.3695 253.1759 0012726 219.5830 140.4467 15.01912704418406
CORVUS BC1
1 42847U 17042Y   25076.46414517 .00008945 00000+0 68285-3 0 9998
2 42847 97.3715 253.6385 0012247 197.7386 162.3413 15.02141936418429
MIRATA
1 43015U 17073C   25076.57954507 .00092555 00000+0 21899-2 0 9999
2 43015 97.5527 328.3987 0107325 30.1811 330.5556 15.35597913397859
MAKERSAT 0
1 43016U 17073D   25076.61044290 .00030692 00000+0 13222-2 0 9999
2 43016 97.5333 315.7349 0158231 70.6784 291.1481 15.11832553397032
SIRION PATHFINDER-2
1 43759U 18099B   25076.58477393 .00011472 00000+0 73759-3 0 9999
2 43759 97.4880 131.5470 0011249 78.2827 281.9663 15.08513700343643
CORVUS BC4
1 43767U 18099K   25076.60212833 .00010603 00000+0 70767-3 0 9998
2 43767 97.4709 127.7631 0010807 127.2363 232.9852 15.07158735343500
MOVE-II
1 43780U 18099Y   25076.62132097 .00120930 00000+0 22968-2 0 9992
2 43780 97.4754 147.7494 0003341 121.5545 238.6032 15.47830130344704
SPACEBEE-7
1 43816U 18099BL 25076.41718690 .00051102 00000+0 17784-2 0 9992
2 43816 97.5052 145.4151 0006897 64.5602 295.6351 15.29499413343903
SHIELDS 1
1 43850U 18104B   25076.55714927 .00042977 00000+0 65379-3 0 9995
2 43850 85.0120 95.4448 0010911 107.7228 252.5223 15.54284930348378
SONATE
1 44400U 19038Q   25076.54158776 .00117359 00000+0 12014-2 0 9991
2 44400 97.7062 94.1030 0009222 178.2536 181.8756 15.64566388316322
DUCHIFAT-3
1 44854U 19089C   25076.60465013 .00067501 00000+0 17857-2 0 9995
2 44854 36.9466 165.8299 0005769 208.1123 151.9320 15.37299378290045

M2 PATHFINDER
1 45727U 20037E   25076.45627367 .00009564 00000+0 74869-3 0 9997
2 45727 97.8054 258.5336 0011900 264.8707 95.1159 15.01188288256888
NETSAT-4
1 46504U 20068U   25076.44475864 .00028471 00000+0 10792-2 0 9999
2 46504 97.8403 49.7535 0010227 124.7580 235.4622 15.26802060245694
NETSAT-3
1 46505U 20068V   25076.42838181 .00026246 00000+0 10302-2 0 9998
2 46505 97.8396 48.8634 0009334 133.4728 226.7287 15.25665761245665
NETSAT-1
1 46506U 20068W   25076.49945818 .00019810 00000+0 87583-3 0 9997
2 46506 97.8418 47.3321 0008130 143.8108 216.3678 15.21714046245563
NETSAT-2
1 46507U 20068X   25076.48138310 .00028455 00000+0 10881-2 0 9999
2 46507 97.8392 49.3291 0007345 143.1537 217.0206 15.26534716245642
WILDTRACKCUBE-SIMBA
1 47941U 21022K   25076.63388640 .00047943 00000+0 12424-2 0 9991
2 47941 97.4315 339.6044 0008384 251.3165 108.7171 15.38846273220254
GRBALPHA
1 47959U 21022AD 25076.57905108 .00147447 00000+0 18200-2 0 9995
2 47959 97.4271 345.4346 0004871 201.1278 158.9778 15.59653553219459
LEDSAT
1 49069U 21073D   25076.57751341 .00073594 00000+0 13831-2 0 9999
2 49069 97.3969 155.3362 0010884 28.3534 331.8306 15.48265524198389
ROBUSTA-1F (MTCUBE 2)
1 53109U 22080E   25076.39163509 -.00000003 00000+0 00000+0 0 9998
2 53109 70.1186 97.1092 0008453 25.9388 334.1695 6.42584398 62712
SITRO-AIS 5 (KATYS)
1 57176U 23091L   25076.61826221 .00018840 00000+0 94408-3 0 9997
2 57176 97.5698 133.5138 0013579 258.7609 101.2099 15.17330654 94839
SITRO-AIS 6 (CHIRKIN)
1 57192U 23091AC 25076.60118858 .00018699 00000+0 93882-3 0 9991
2 57192 97.5694 133.5197 0013460 258.6490 101.3231 15.17266075 94838
SITRO-AIS 8 (ANOKHIN)
1 57193U 23091AD 25076.58003619 .00021220 00000+0 10309-2 0 9993
2 57193 97.5690 133.8399 0013200 258.4179 101.5574 15.18392396 94857
SITRO-AIS 7 (FARTUSHNIY)
1 57194U 23091AE 25076.61802065 .00019381 00000+0 97476-3 0 9996
2 57194 97.5695 133.4870 0013361 259.4503 100.5225 15.17198766 94837
SITRO-AIS 10 (BURDAEV)

1 57199U 23091AK 25076.60361417 .00024233 00000+0 10829-2 0 9999
2 57199 97.5701 135.7666 0009169 239.9816 120.0510 15.21292443 94970
SITRO-AIS 9 (SHCHUKIN)
1 57201U 23091AM 25076.61244454 .00023723 00000+0 10641-2 0 9990
2 57201 97.5698 135.7149 0009105 240.1908 119.8423 15.21168930 94973
SITRO-AIS 12 (SMIRENNIY)
1 57204U 23091AQ 25076.60569378 .00024304 00000+0 10837-2 0 9990
2 57204 97.5706 135.9533 0009192 233.7786 126.2600 15.21366050 94986
SITRO-AIS 11 (SHEFFER)
1 57208U 23091AU 25076.56857806 .00025934 00000+0 11505-2 0 9998
2 57208 97.5705 135.9835 0009030 234.2219 125.8178 15.21528918 94980
VERONIKA
1 58261U 23174F   25076.48473671 .00106111 00000+0 18961-2 0 9995
2 58261 97.4216 158.9450 0005628 338.5307 21.5707 15.49630102 75572
ROBUSTA-1E (ENSO)
1 58470U 23185J   25076.56875545 .00069284 00000+0 14497-2 0 9993
2 58470 97.3826 149.5916 0007315 29.1090 331.0565 15.45191651 72014
SITRO-AIS 29
1 59052U 24039B   25076.58055342 .00217893 00000+0 19240-2 0 9998
2 59052 97.4148 48.8913 0002456   0.7038 359.4226 15.68001023 58745
SITRO-AIS 30
1 59053U 24039C   25076.60059566 .00205787 00000+0 19490-2 0 9990
2 59053 97.4147 48.6971 0003176 347.0802 13.0376 15.66293161 58724
SITRO-AIS 31
1 59054U 24039D   25076.58837521 .00214816 00000+0 19411-2 0 9999
2 59054 97.4161 48.8831 0002931 357.9798   2.1450 15.67438212 58754
SITRO-AIS 33
1 59055U 24039E   25076.49233792 .00202171 00000+0 18123-2 0 9990
2 59055 97.4145 48.8610 0002498   0.4341 359.6921 15.67676011 58736
SITRO-AIS 35
1 59056U 24039F   25076.60464888 .00222445 00000+0 19597-2 0 9998
2 59056 97.4161 49.0209 0002741   8.0765 352.0540 15.68043257 58754
SITRO-AIS 32
1 59057U 24039G   25076.61269238 .00200597 00000+0 18654-2 0 9999
2 59057 97.4162 48.8658 0002930 357.8795   2.2452 15.66767521 58749
SITRO-AIS 34
1 59058U 24039H   25076.49416544 .00215407 00000+0 19366-2 0 9997
2 59058 97.4149 48.8633 0002566   3.9608 356.1672 15.67562935 58732

Starlink(Limited to 100)

```
STARLINK-1008
1 44714U 19074B   25073.10951218  .00021645  00000+0  14688-2 0  9991
2 44714  53.0556   5.3233 0001425 110.3415 249.7727 15.06367812294573
STARLINK-1010
1 44716U 19074D   25073.18323696  .00030327  00000+0  20475-2 0  9992
2 44716  53.0552   4.9934 0001824  80.0165 280.1030 15.06374388294563
STARLINK-1011
1 44717U 19074E   25073.18138816  .00018961  00000+0  12894-2 0  9997
2 44717  53.0549  25.0025 0001244  72.5435 287.5690 15.06370052294306
STARLINK-1012
1 44718U 19074F   25073.22009615  .00005332  00000+0  37668-3 0  9992
2 44718  53.0555   4.8230 0001656 104.9947 255.1225 15.06390126294581
STARLINK-1013
1 44719U 19074G   25073.09478412  .00017335  00000+0  11803-2 0  9991
2 44719  53.0560   5.3894 0001471  74.9806 285.1346 15.06384437294568
STARLINK-1014
1 44720U 19074H   25073.25002315  .00342484  00000+0  66020-2 0  9993
2 44720  53.0495 337.2331 0012776 144.3676 326.8950 15.46003222294981
STARLINK-1015
1 44721U 19074J   25073.20170887  .00027915  00000+0  18871-2 0  9999
2 44721  53.0554   5.2598 0001578  71.1761 288.9399 15.06368686294579
STARLINK-1017
1 44723U 19074L   25073.18691759  .00027762  00000+0  18768-2 0  9999
2 44723  53.0541   4.9763 0001297  77.6183 282.4951 15.06370398294581
STARLINK-1019
1 44724U 19074M   25073.08371360  .00019228  00000+0  13069-2 0  9999
2 44724  53.0546   5.4402 0001238  71.6055 288.5068 15.06380632294566
STARLINK-1020
1 44725U 19074N   25072.89019633 -.00000323  00000+0 -27785-5 0  9991
2 44725  53.0558  26.3108 0001443  89.3707 270.7447 15.06393004294081
STARLINK-1021
1 44726U 19074P   25072.94734972 -.00001539  00000+0 -84501-4 0  9996
2 44726  53.0550   6.0519 0001542  80.5228 279.5935 15.06377398294375
STARLINK-1027
1 44732U 19074V   25073.25002315  .00327453  00000+0  18046-2 0  9990
2 44732  53.0532 356.0697 0008619  97.5572 205.8998 15.78186112294719
```

```
STARLINK-1029
1 44734U 19074X   25072.82568176 -.00005916  00000+0 -37870-3 0  9992
2 44734  53.0531 286.6003 0001442  86.1690 273.9464 15.06390225295450
STARLINK-1030
1 44735U 19074Y   25073.15190424  .00016607  00000+0  11320-2 0  9995
2 44735  53.0553  25.1329 0001311  81.5965 278.5173 15.06372898294296
STARLINK-1031
1 44736U 19074Z   25073.16665264  .00011655  00000+0  80093-3 0  9998
2 44736  53.0566  25.0704 0001824  86.2608 273.8590 15.06358500294309
STARLINK-1032
1 44737U 19074AA  25072.91668981  .00347204  56524-4  10565-2 0  9995
2 44737  53.0428 333.7455 0006391 148.6727   4.7046 15.91501769  6093
STARLINK-1035
1 44740U 19074AD  25073.25002315  .00374750  00000+0  14831-2 0  9999
2 44740  53.0482 352.3547 0006854 108.9921  70.2182 15.85220334294766
STARLINK-1036
1 44741U 19074AE  25072.85333472 -.00006605  00000+0 -42504-3 0  9998
2 44741  53.0547  26.4704 0001543  99.9988 260.1175 15.06389907294087
STARLINK-1039
1 44744U 19074AH  25073.17955456  .00000663  00000+0  63429-4 0  9995
2 44744  53.0555  45.0071 0001373  92.4782 267.6364 15.06384572294023
STARLINK-1042
1 44747U 19074AL  25073.09831233  .00026533  00000+0  79604-3 0  9990
2 44747  53.0519   3.0718 0006034  96.9074 263.2614 15.34288874294625
STARLINK-1043
1 44748U 19074AM  25073.22377316 -.00004035  00000+0 -25224-3 0  9997
2 44748  53.0547  44.8108 0001529  84.0381 276.0783 15.06384277294033
STARLINK-1046
1 44751U 19074AQ  25073.17217266 -.00003161  00000+0 -19346-3 0  9999
2 44751  53.0540  45.0382 0001479  87.8433 272.2726 15.06387103294025
STARLINK-1047
1 44752U 19074AR  25073.11290710  .00088789  00000+0  39159-2 0  9999
2 44752  53.0545  17.4996 0004166  93.1472 267.0000 15.21035298294405
STARLINK-1048
1 44753U 19074AS  25073.19798887 -.00002178  00000+0 -12742-3 0  9996
2 44753  53.0564   4.9267 0001444 100.6884 259.4268 15.06389871294588
STARLINK-1052
1 44757U 19074AW  25072.97438382  .02309016  74266-2  16880-2 0  9991
2 44757  53.0126 279.7539 0005184 260.5408 210.0644 16.16847824295753
STARLINK-1053
```

```
1 44758U 19074AX  25072.91668981  .00362730  00000+0  93585-2 0  9995
2 44758  53.0474  34.7692 0001305  85.2150 233.2607 15.37207854  5891
STARLINK-1054
1 44759U 19074AY  25073.13530799  .00001127  00000+0  94535-4 0  9994
2 44759  53.0546  45.2079 0001506 108.9632 251.1520 15.06396224294023
STARLINK-1056
1 44761U 19074BA  25073.19797543 -.00000786  00000+0 -33859-4 0  9999
2 44761  53.0542  44.9253 0001527  91.3207 268.7957 15.06389097294037
STARLINK-1057
1 44762U 19074BB  25072.86808673  .00001036  00000+0  88465-4 0  9990
2 44762  53.0560  26.4054 0001622  89.8552 270.2623 15.06394380294087
STARLINK-1058
1 44763U 19074BC  25072.91668981  .00377291  00000+0  12341-2 0  9990
2 44763  53.0444 356.4780 0005169 163.3238 246.8833 15.89109721  6076
STARLINK-1060
1 44765U 19074BE  25073.08186865 -.00002281  00000+0 -13432-3 0  9996
2 44765  53.0549  25.4437 0001569 104.6140 255.5024 15.06386543294285
STARLINK-1062
1 44767U 19074BG  25072.91668981  .00504449  11208-3  13854-2 0  9997
2 44767  53.0401 355.1429 0003385 139.7651 239.5365 15.93445239  6074
STARLINK-1063
1 44768U 19074BH  25073.22746654 -.00001080  00000+0 -53625-4 0  9998
2 44768  53.0555  44.7941 0001516  92.2201 267.8962 15.06387280294030
STARLINK-1067
1 44771U 19074BL  25073.21640975 -.00002089  00000+0 -12144-3 0  9990
2 44771  53.0549  44.8415 0001485  77.0531 283.0623 15.06382937294034
STARLINK-1068
1 44772U 19074BM  25073.14084388 -.00005806  00000+0 -37137-3 0  9992
2 44772  53.0571  25.1840 0001650 105.1145 255.0027 15.06379671294298
STARLINK-1073
1 44914U 20001A   25073.25002315  .00194318  00000+0  95651-3 0  9994
2 44914  53.0455 121.4369 0008372  26.4040  46.1457 15.81043503286124
STARLINK-1098
1 44917U 20001D   25072.65981607  .00026594  00000+0  17946-2 0  9990
2 44917  53.0537 167.3457 0001391  91.1400 268.9748 15.06460964285439
STARLINK-1102
1 44920U 20001G   25073.20292579  .01669586  25404-2  11030-2 0  9990
2 44920  53.0274   9.3887 0003908 183.7204 327.2506 16.17060710287700
STARLINK-1103
1 44921U 20001H   25072.91668981  .01366321  00000+0  95313-2 0  9991
```

2 44921 53.0481 130.5171 0000645 65.9899 110.1014 15.71307541 6044
STARLINK-1104
1 44922U 20001J   25072.54186733 .00012490 00000+0 85523-3 0 9998
2 44922 53.0541 167.8742 0001410 97.4051 262.7099 15.06429656285417
STARLINK-1106
1 44923U 20001K   25073.25002315 .00212394 00000+0 12691-2 0 9991
2 44923 53.0023 39.8839 0007282 56.7617 269.8149 15.76704765287259
STARLINK-1112
1 44925U 20001M   25073.23482865 -.00001586 00000+0 -87630-4 0 9991
2 44925 53.0534 164.7643 0001635 103.4193 256.6978 15.06394502285512
STARLINK-1114
1 44927U 20001P   25073.24589837 .00022034 00000+0 14933-2 0 9994
2 44927 53.0527 164.7123 0001009 115.9236 244.1857 15.06404659285524
STARLINK-1123
1 44930U 20001S   25072.53080842 .00011434 00000+0 78463-3 0 9992
2 44930 53.0518 167.9250 0000884 93.0166 267.0924 15.06429194285410
STARLINK-1130 (DARKSAT)
1 44932U 20001U   25072.42635579 .00109973 00000+0 10222-2 0 9999
2 44932 53.0488 130.5327 0005743 18.8430 341.2796 15.66587950287164
STARLINK-1144
1 44933U 20001V   25072.52686508 .00064281 00000+0 26791-2 0 9999
2 44933 53.0535 157.2795 0004261 357.2853   2.8119 15.23121001286854
STARLINK-1071
1 44934U 20001W   25073.22192356 .00003898 00000+0 28033-3 0 9990
2 44934 53.0544 144.8230 0002340 56.2371 303.8841 15.06415529285798
STARLINK-1079
1 44937U 20001Z   25072.91668981 .00166715 00000+0 27246-2 0 9992
2 44937 53.0414 95.3105 0002528 301.2845 69.0104 15.51474604 5977
STARLINK-1091
1 44940U 20001AC 25072.52159991 .00022037 00000+0 14918-2 0 9999
2 44940 53.0547 147.9660 0001523 92.2588 267.8576 15.06447819285680
STARLINK-1094
1 44941U 20001AD 25072.61006147 .00028672 00000+0 19324-2 0 9991
2 44941 53.0540 147.5664 0001510 92.4639 267.6523 15.06468164285708
STARLINK-1096
1 44942U 20001AE 25073.10540444 .00059191 00000+0 90999-3 0 9998
2 44942 53.0044   6.3190 0004551 68.2625 291.8868 15.53687705287729
STARLINK-1109
1 44945U 20001AH 25072.91668981 .00180278 00000+0 12900-2 0 9992
2 44945 53.0453 101.4036 0006493 36.0056 334.8924 15.72651039 5989

```
STARLINK-1122
1 44949U 20001AM  25073.22930538 -.00002904  00000+0 -17618-3 0  9994
2 44949  53.0541 144.7895 0000413  26.3732 333.7278 15.06393624285792
STARLINK-1117
1 44952U 20001AQ  25073.25002315  .00138585  00000+0  12413-2 0  9994
2 44952  53.0471 132.8077 0003452  32.8172  87.9917 15.67404158285963
STARLINK-1066
1 44954U 20001AS  25073.17584726  .00000134  00000+0  27905-4 0  9990
2 44954  53.0537 125.0293 0001751  76.6276 283.4908 15.06403819286019
STARLINK-1076
1 44959U 20001AX  25072.86092118  .00702096  24368-3  11592-2 0  9995
2 44959  53.0401  79.4460 0007516  41.2922  29.8750 16.02498936286662
STARLINK-1080
1 44961U 20001AZ  25073.16110987 -.00004608  00000+0 -29063-3 0  9999
2 44961  53.0544 125.0954 0001407  76.3583 283.7563 15.06401247286074
STARLINK-1088
1 44966U 20001BE  25072.91668981  .00269642  00000+0  12785-2 0  9999
2 44966  53.0560 359.4059 0001882  83.4520 307.5306 15.81684541  5996
STARLINK-1090
1 44968U 20001BG  25073.16479413 -.00000515  00000+0 -15653-4 0  9992
2 44968  53.0540 125.0779 0001635  99.0227 261.0947 15.06404745286073
STARLINK-1092
1 44969U 20001BH  25072.91668981  .01306600  00000+0  22326-1 0  9990
2 44969  53.0491 112.8890 0001118  88.0358 359.9640 15.47791408  5948
STARLINK-1093
1 44970U 20001BJ  25072.35711312  .00101953  00000+0  10963-2 0  9995
2 44970  53.0465  94.8246 0003242   8.1388 351.9678 15.62960586286419
STARLINK-1107
1 44972U 20001BL  25073.24567054  .00066336  00000+0  22240-2 0  9994
2 44972  53.0240 106.3638 0004249  30.7809 329.3438 15.30306643286341
STARLINK-1115
1 44973U 20001BM  25072.44388164  .00042646  00000+0  93304-3 0  9997
2 44973  53.0417  94.8091 0007766 346.6650  13.4149 15.43716827286435
STARLINK-1132
1 45044U 20006A   25073.19059366 -.00001060  00000+0 -52251-4 0  9998
2 45044  53.0538  84.9582 0001318 114.3057 245.8070 15.06397972282741
STARLINK-1131
1 45047U 20006D   25073.23304960  .00000870  00000+0  77314-4 0  9992
2 45047  53.0526 105.3085 0001268 112.1755 247.9368 15.06401263282463
STARLINK-1134
```

```
1 45048U 20006E   25073.11521161  .00011169  00000+0  68796-3 0  9990
2 45048  53.0525 103.8347 0000763   1.3166 358.7827 15.10444163282474
STARLINK-1148
1 45052U 20006J   25072.91668981  .00095736  00000+0  15064-2 0  9995
2 45052  53.0497  65.4626 0007545  14.8640 228.5309 15.52815947  5976
STARLINK-1156
1 45054U 20006L   25072.47369785  .00001312  00000+0  10691-3 0  9997
2 45054  53.0533 108.1776 0001331  90.4154 269.6987 15.06407699282017
STARLINK-1159
1 45057U 20006P   25072.35573016  .00008496  00000+0  58831-3 0  9999
2 45057  53.0518 108.7068 0001696  98.9253 261.1928 15.06417223282342
STARLINK-1162
1 45058U 20006Q   25073.25002315  .00219048  00000+0  12639-2 0  9991
2 45058  53.0448  75.3882 0008412  34.9729 234.9476 15.77463357282881
STARLINK-1166
1 45060U 20006S   25073.22931041  .00001846  00000+0  14280-3 0  9998
2 45060  53.0529 104.7873 0001286  92.2584 267.8552 15.06400026282470
STARLINK-1169
1 45061U 20006T   25073.23667269 -.00002833  00000+0 -17137-3 0  9991
2 45061  53.0537 104.7559 0001539  62.7474 297.3672 15.06394576282475
STARLINK-1171
1 45062U 20006U   25073.22194860  .00003569  00000+0  25838-3 0  9995
2 45062  53.0526 104.8195 0001499  88.1345 271.9816 15.06398795282470
STARLINK-1133
1 45064U 20006W   25073.23483773 -.00000092  00000+0  12713-4 0  9990
2 45064  53.0546  84.7598 0001390  97.3444 262.7703 15.06389829282762
STARLINK-1150
1 45067U 20006Z   25073.22747578  .00003098  00000+0  22686-3 0  9995
2 45067  53.0521  84.7948 0001454  90.6514 269.4641 15.06391483282755
STARLINK-1161
1 45068U 20006AA  25073.25002315  .00161586  00000+0  31642-2 0  9990
2 45068  53.0291  56.1288 0006030  70.5947 235.7013 15.46319870283150
STARLINK-1167
1 45071U 20006AD  25073.19428642 -.00001152  00000+0 -58453-4 0  9997
2 45071  53.0547  84.9458 0001528 108.0187 252.0968 15.06393904282747
STARLINK-1168
1 45072U 20006AE  25073.19798096 -.00001108  00000+0 -55488-4 0  9997
2 45072  53.0536  84.9280 0001454  90.9970 269.1186 15.06386090282756
STARLINK-1170
1 45073U 20006AF  25073.21213749  .00127523  00000+0  10920-2 0  9996
```

2 45073 53.0535 76.2421 0001497 92.8413 267.2774 15.68553330282862
STARLINK-1172
1 45074U 20006AG 25073.20904035 -.00001867 00000+0 -10648-3 0 9993
2 45074 53.0536 84.8785 0001763 92.0391 268.0799 15.06383940282759
STARLINK-1174
1 45075U 20006AH 25072.91668981 .00200964 00000+0 13483-2 0 9994
2 45075 53.0533 76.8274 0002261 98.1274   7.6309 15.74111037 5817
STARLINK-1153
1 45080U 20006AN 25073.18691417 -.00000460 00000+0 -12002-4 0 9999
2 45080 53.0541 84.9774 0001327 93.9368 266.1773 15.06391575282407
STARLINK-1151
1 45081U 20006AP 25073.23853978 .00001753 00000+0 13659-3 0 9990
2 45081 53.0529 84.8211 0001485 96.8974 263.2184 15.06392648282764
STARLINK-1190
1 45083U 20006AR 25073.11874572 .00001791 00000+0 13913-3 0 9997
2 45083 53.0537 105.2822 0001538 91.9484 268.1681 15.06392460282456
STARLINK-1173
1 45084U 20006AS 25073.23300196 .00000485 00000+0 51452-4 0 9997
2 45084 53.0550 64.7692 0001566 89.5987 270.5182 15.06390926283143
STARLINK-1179
1 45085U 20006AT 25073.22931799 .00002330 00000+0 17535-3 0 9990
2 45085 53.0531 64.7852 0001279 86.7743 273.3393 15.06373606283030
STARLINK-1185
1 45087U 20006AV 25072.68379982 .00001975 00000+0 15149-3 0 9994
2 45087 53.0537 67.2360 0001444 92.3164 267.7991 15.06393255282610
STARLINK-1183
1 45088U 20006AW 25073.23669905 -.00005314 00000+0 -33847-3 0 9992
2 45088 53.0528 64.7535 0001610 104.1367 255.9801 15.06357368282691
STARLINK-1176
1 45090U 20006AY 25073.22099463 -.00000351 00000+0 -46768-5 0 9994
2 45090 53.0549 64.8152 0001356 86.1897 273.9247 15.06385719282692
STARLINK-1137
1 45092U 20006BA 25072.98252664 .00244475 00000+0 11224-2 0 9993
2 45092 53.0518 53.4998 0000808 97.1668   6.3010 15.82446460283176
STARLINK-1142
1 45093U 20006BB 25072.97084109 .00049323 00000+0 20983-2 0 9997
2 45093 53.0479 53.7555 0004095 71.9677 288.1764 15.22548123282827
STARLINK-1146
1 45094U 20006BC 25073.20625122 -.00001082 00000+0 -53783-4 0 9999
2 45094 53.0582 64.8821 0001809 102.8736 257.2455 15.06382100283044

```
STARLINK-1147
1 45095U 20006BD  25073.19988609 -.00001541  00000+0 -84588-4 0  9997
2 45095  53.0537  65.4948 0001419  95.1633 264.9518 15.06389990283037
STARLINK-1152
1 45096U 20006BE  25073.25656729  .00012838  00000+0  81463-3 0  9997
2 45096  53.0539  63.8289 0002276  33.4795 326.6338 15.09224375283052
STARLINK-1184
1 45098U 20006BG  25073.18508233  .00000837  00000+0  75103-4 0  9998
2 45098  53.0559  64.9835 0001618  88.2406 271.8769 15.06388364281234
STARLINK-1193
1 45100U 20006BJ  25073.24774607  .00002018  00000+0  15437-3 0  9995
2 45100  53.0537  64.7024 0001443  96.6636 263.4518 15.06391752283041
STARLINK-1143
1 45179U 20012B   25072.71351297  .00083993  00000+0  43386-2 0  9999
2 45179  53.0509 224.5296 0008281 162.5784 197.5495 15.15553406280467
STARLINK-1200
1 45181U 20012D   25072.74275256 -.00004249  00000+0 -26662-3 0  9993
2 45181  53.0535 226.9694 0001554 107.7624 252.3534 15.06389938280435
STARLINK-1201
1 45182U 20012E   25072.63032981  .00005966  00000+0  41906-3 0  9991
2 45182  53.0526 207.4744 0001503  78.5417 281.5740 15.06398754280546
STARLINK-1202
1 45183U 20012F   25072.71328392  .00005205  00000+0  36806-3 0  9994
2 45183  53.0546 227.1052 0001146  68.0952 292.0159 15.06396479280432
```